

Metallic MoS₂ for High Performance Energy Storage and Energy Conversion

Yucong Jiao, Ahmed M. Hafez, Daxian Cao, Alolika Mukhopadhyay, Yi Ma, and Hongli Zhu*

Metallic phase 2D molybdenum disulfide (MoS₂) is an emerging class of materials with remarkably higher electrical conductivity and catalytic activities. The goal of this study is to review the atomic structures and electrochemistry of metallic MoS₂, which is essential for a wide range of existing and new enabling technologies. The scope of this paper ranges from the atomic structure, band structure, electrical and optical properties to fabrication methods, and major emerging applications in electrochemical energy storage and energy conversion. This paper also thoroughly covers the atomic structure–properties–application relationships of metallic MoS₂. Understanding the fundamental properties of these structures is crucial for designing and manufacturing products for emerging applications. Today, a more holistic understanding of the interplay between the structure, chemistry, and performance of metallic MoS₂ is advancing actual applications of this material. This new level of understanding also enables a myriad of new and exciting applications, which motivated this review. There are excellent reviews already on the traditional semiconducting MoS₂, and this review, for the first time, focuses on the uniqueness of conducting metallic MoS₂ for energy applications and offers brand new materials for clean energy application.

1. Introduction


Layered transition metal dichalcogenides (TMD) have attracted widespread attention due to their remarkable physical, chemical, electronic, and optical properties, which endow them as good candidates for energy storage and conversion. But most of the current reported TMDs show poor electronic conductivity.^[1–10] Recently, one typical layered transition metal dichalcogenide material, molybdenum disulfide (MoS₂) with weakly coupled layers, where a layer of Mo atoms is sandwiched between two layers of S atoms, has attracted broad interest as a promising TMD on energy storage and conversion fields, owing to its intrinsic bandgap, unique layered structure, and catalytic activity.^[11–19] There are different kinds of poly-types of MoS₂ structures with different coordinates of Mo and S atoms: 1T

MoS₂, 2H MoS₂, and 3R MoS₂.^[20,21] The 1T phase has coordinately octahedral structure with Mo atom exposed to the surface, and one S–Mo–S layer per unit cell. Both the 2H (with two S–Mo–S layers per elemental cell) and 3R MoS₂ phases (with three S–Mo–S unites) are trigonal prismatic structures, and own the S coordination opposed to the 1T octahedral coordination. But the stacking order between 2H and 3R is different, where the 2H is AbA, BaB, AbA, and 3R is AbA, BcB, CaC, AbA. Furthermore, the 3R phase is metastable and can be easily transferred to 2H phase, which decreases its competitiveness on energy storage fields, compared to 2H phase.^[21]

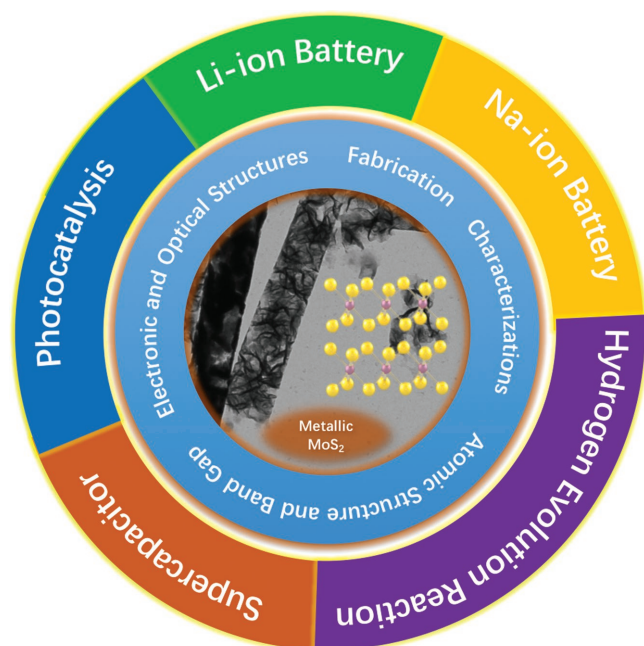
The main two MoS₂ phases, metallic 1T phase and semiconducting 2H phase, due to the distinct structures, exhibit noticeable difference in their physical and chemical properties, especially the conductivity properties, where the metallic phase has $\approx 10^5$ times electrical conductivity compared to the semiconducting phase.^[22] The

low electrical conductivity of semiconducting MoS₂ is disadvantageous for electrochemical energy storage.^[23,24] However, due to its high stability and well-developed synthesis approach, 2H MoS₂ is still the most popular MoS₂ phase on energy storage and conversion fields in most of the studies nowadays.^[18,25–27] Therefore, in order to facilitate the electron transport in the 2H MoS₂ electrode for its application in energy storage and conversion, additional conductive additives such as graphene, carbon nanotubes, and carbon black are usually necessary to attend, which increase its cost, limit the rate performance, and decrease the active material loading. Compared to the 2H phase of the MoS₂, the 1T phase has superior electron transfer capability due to its significantly (10^5 times) higher electronic conductivity.^[28] Consequently, using 1T MoS₂ as an electrode will minimize or even eliminate the addition of any further conductive additives and simultaneously achieve an excellent rate performance on energy storage fields.^[22,29–32] Furthermore, previous studies found that the basal plane of semiconducting 2H phase MoS₂ is catalytically inert for hydrogen evolution reaction (HER), whereas the basal planes of metallic 1T MoS₂ are rich in active sites,^[33,34] which has the benefit of higher reaction kinetics between electrons and protons (H⁺) on the active sites, and makes the 1T MoS₂ more promising candidate on energy generation and conversion fields. Methods for re-engineering MoS₂ through new metallic

Dr. Y. Jiao, A. M. Hafez, D. Cao, A. Mukhopadhyay, Y. Ma, Prof. H. Zhu
Department of Mechanical and Industrial Engineering
Northeastern University
Boston, MA 02115, USA
E-mail: h.zhu@neu.edu

 The ORCID identification number(s) for the author(s) of this article can be found under <https://doi.org/10.1002/sml.201800640>.

DOI: 10.1002/sml.201800640



Scheme 1. The illustration of metallic MoS₂ structure properties and their potential applications.^[30,36,37]

structures that can solve the intrinsic problems of conductivity and catalytic activities have been developed.^[22,29,35]

In this review, we focus on providing the overview of metallic MoS₂ on the atomic structure, physical and chemical properties, fabrication, characterization, energy storage, and conversation applications (**Scheme 1**). We summarized most of the recent researches in these fields for metallic MoS₂ and particularly emphasized the identification of metallic MoS₂ and semiconducting MoS₂ by their characteristic differences such as atomic structure, bandgap, optical properties, Raman spectra, X-ray Diffraction (XRD), X-ray photoelectron spectroscopy (XPS), etc. In addition, we also highlighted the high conductivity and the performance superiority of metallic MoS₂ electrode on lithium-ion and sodium-ion batteries, supercapacitors, and HER applications. This highly conductive MoS₂ will combine the advantages of the individual building blocks while eliminating the associated shortcomings, leading to expansion of current energy storage technologies. Although there are already some excellent reviews about MoS₂-based materials for energy storage and conversion,^[10,19,20] to the best of our knowledge, there are presently no reviews on metallic MoS₂ for energy storage and energy conversion. We believe that a timely review of this important research will be a valuable resource for this new field, which is rapidly expanding in terms of both scope and interest from the scientific community. Furthermore, this review will accelerate the investigation of metallic conducting MoS₂ with large electron density and build the fundamental knowledge needed to advance its application to various challenges in energy storage and clean energy conversion.

2. Atomic Structure and Bandgap

According to the different Mo atom coordinate phases in a single layer, there are different MoS₂ structures: hexagonal



Yucong Jiao is currently a postdoc at the department of mechanical engineering at Northeastern University. Yucong Jiao received his B.S. degree in polymer science at Zhejiang University, and received his Ph.D. degree in macromolecular science from Fudan University in 2015. His research is concentrated on inorganic nanoparticles self-assembly, and metallic TMDs application on energy storage and conversion.



Ahmed M. Hafez is currently a Ph.D. student at the mechanical engineering department at Northeastern University. He received his B.S. in electrical engineering, then obtained his M.S. in engineering physics from Cairo University in 2016. His research involves developing and investigating nanostructured materials for energy generation and storage both experimentally, and theoretically using DFT calculations. Before joining Northeastern, he joined EML at AUC Egypt in 2014, with research scope on hydrogen evolution and storage. After that, he joined ONE lab at MIT as a visiting student in 2016, with focus on utilizing nanostructured materials in perovskite solar cells fabrication.



Hongli Zhu is currently an assistant professor at Northeastern University. Her group focuses on the research of energy storage, advanced manufacturing, and multi-functional materials. From 2012–2015, she worked at the University of Maryland as a postdoc, focusing on the research of nanopaper electronics and energy storage. From 2009 to 2011, she conducted research on materials science and processing of biodegradable and renewable biomaterials from natural wood in the KTH Royal Institute of Technology in Sweden. Her expertise is on the research of environmentally friendly natural biomaterials and energy storage; design and application of novel transparent nanostructured paper for flexible electronics.

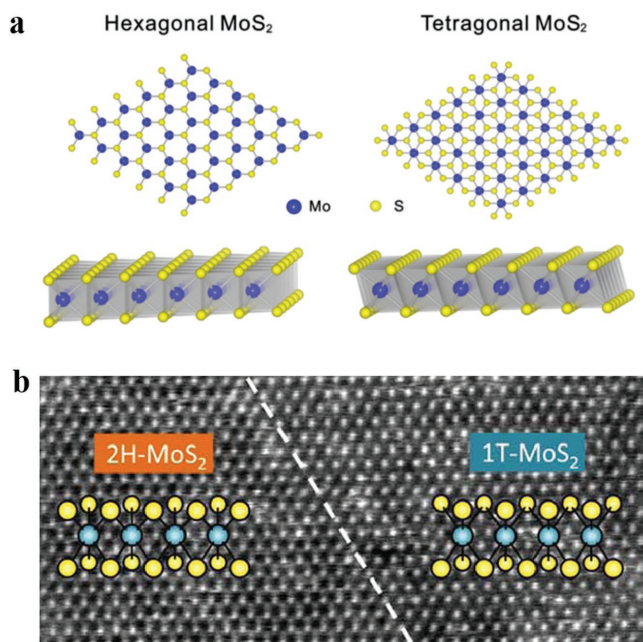


Figure 1. a) Schematic atom structure of different polytypes MoS₂, hexagonal MoS₂, and tetragonal MoS₂. Reproduced with permission.^[38] Copyright 2016, Elsevier. b) Corresponding STEM images of semiconducting MoS₂ (2H MoS₂) and metallic MoS₂ (1T MoS₂). Reproduced with permission.^[36] Copyright 2012, American Chemical Society.

MoS₂ and tetragonal MoS₂ (Figure 1a).^[38,39] In 2H MoS₂ (semiconducting phase), the Mo atom layer in hexagonal MoS₂ is

sandwiched between S layers with a trigonal prismatic coordination of Mo atom.^[40–44] By contrast, the tetragonal MoS₂, marked as ordered 1T MoS₂ or distorted 1T' MoS₂ (metallic phase), has an octahedral coordination of Mo atoms.^[45–48] Based on this structural difference, the semiconducting and metallic MoS₂ exhibit different properties, which has been discussed elaborately in the following paragraphs. Figure 1b shows the scanning transmission electron microscope (STEM) image of the corresponding Mo arrangement of trigonal prismatic 2H MoS₂ and octahedral 1T MoS₂.^[36] As the transmission electron microscopy (TEM) images shown in Figure 1b, the lattice array of metallic phase is hexagonal, but the semiconducting phase owns a honeycomb-like lattice with minor variation in intensity contrast between two adjacent sites.

Metallic MoS₂ does not exist in nature. People usually use butyllithium to intercalate semiconducting MoS₂ with Li-ion and obtain metastable metallic MoS₂. However, the metastable metallic MoS₂ regains its semiconducting phase after Li-ion deintercalation from the MoS₂. To gain more insights on the structure of various phases of MoS₂, the geometrical structures of the 2H phase with a trigonal prism, 1T phase, and 1T' phase with octahedral coordination are shown in Figure 2.^[46] Subsequently, different polytypes of MoS₂ own significantly different electronic properties due to their different Mo–S atom arrangements and bandgap. Trigonal prismatic monolayer 2H MoS₂ is a semiconducting material.^[49] The Mo 4d orbitals are divided into three degenerate states, where the energy gap is 1.0 eV. Further, the 4d₂₂ orbital is occupied by two d electrons of Mo⁴⁺ species that lead to the semiconductivity.^[20] The indirect bandgap of semiconducting

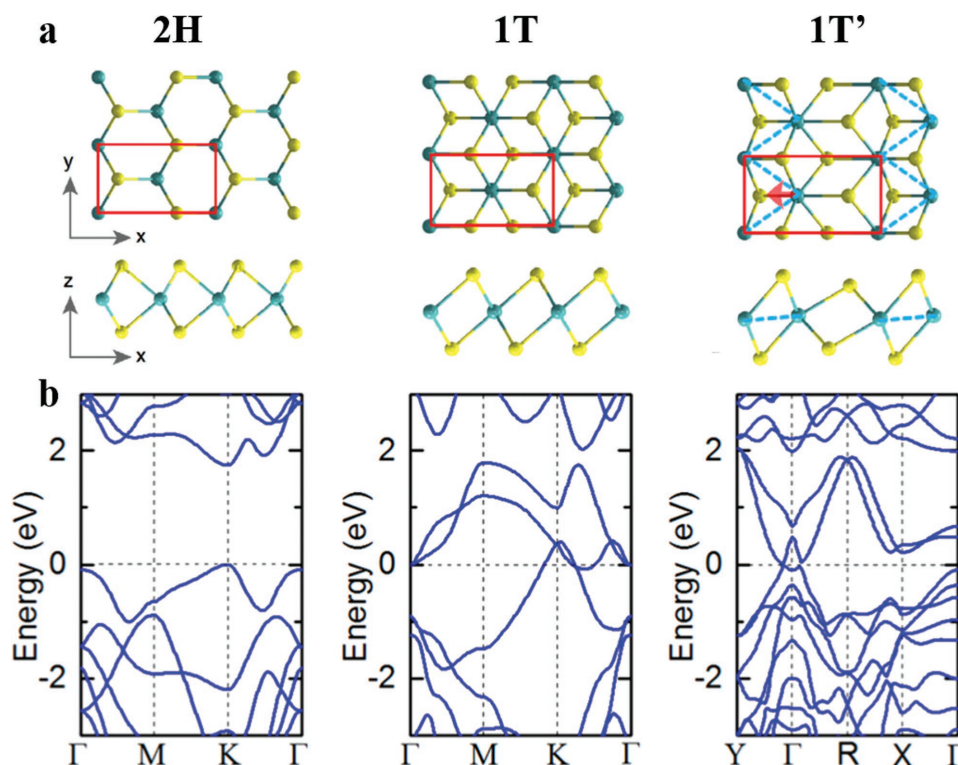


Figure 2. a) 2D view of the geometrical structures of 2H, 1T, and 1T' MoS₂. b) Coordinate band structures. Reproduced with permission.^[46] Copyright 2015, American Chemical Society. Reproduced with permission.^[54] Copyright 2014, Science. Cyan, Mo; yellow, S.

MoS₂ is around 1.9 eV, as shown in Figure 2b.^[46,50–52] By contrast, 1T MoS₂ is a paramagnetic and metallic material. From the atomic structure, the 1T MoS₂ is a standard 2 × 1 superlattice structure in the *x* direction. The d orbitals of the octahedral ligands field are degenerated in tetragonal symmetry and can be filled by up to six electrons for metallic phase structure.^[20,53] As a result, the bandgap of metallic MoS₂ is negligible as shown in Figure 2b. Correspondingly, in the 1T' MoS₂, the Mo atoms are distorted with 1D zigzag chains along the *y* direction and possess a bandgap of 0.006 eV (Figure 2b). The energy state of 1T' MoS₂ is 0.15 eV lower per MoS₂ unit compared to 1T MoS₂ phase.^[46] Li and co-workers^[54] also concluded that there was no energy barrier from 1T to 1T', which implied that there would be spontaneous structural relaxation of 1T to 1T' in monolayer MoS₂. To simply identify the 1T and 1T', researchers have already reported this by STEM method, where they proved that the 1T' structure consisted Mo zigzag chains from STEM images.

3. Electronic and Optical Properties

Semiconducting MoS₂ and metallic MoS₂ exhibit different electronic and optical properties due to the different atomic structures.^[55–58] Semiconducting MoS₂ exhibits characteristic optical peaks due to its photoluminescence energy of ≈1.9 eV, consistent with its bandgap energy.^[59–61] As the ultraviolet–visible spectroscopy spectra shown in Figure 3a, the semiconducting phase (red curve, solution exfoliated) owns two notable peaks at 604 and 667 nm, related to the direct-gap transition.^[62] By contrast, no visible peaks appeared at 604 and 667 nm for metallic MoS₂, as the bandgap energy is different for metallic MoS₂ compared to the semiconducting phase of MoS₂^[50,63] (black curve, electrochemically exfoliated) in Figure 3a). The metallic MoS₂ and semiconducting MoS₂ can also be distinguished by prominent differences in their appearance. The dispersion of semiconducting phase of MoS₂ is dark yellow or green, whereas the color of the metallic

phase is dark grey^[62] (inset image in Figure 3a). Figure 3b is another optical absorption spectra for metallic and semiconducting phase MoS₂.^[28] The semiconducting phase owns two absorption peaks at 613 and 660 nm, relevant to the energy split of valence band spin–orbital coupling.^[23] By contrast, the optical absorption spectrum of metallic phase (red curve in Figure 3b) does not contain any peak, corresponding to the result of Figure 3a. The inset image also confirms the difference between a metallic MoS₂ solution and semiconducting MoS₂ solution. The color for metallic phase is grey, whereas the semiconducting phase is green.^[28]

4. Fabrication Methods for Metallic MoS₂

To obtain high purity metallic MoS₂, the fabrication method is the first and most important step. Usually, there are two kinds of fabrication methods: a top-down approach such as bulk MoS₂ exfoliation; and a bottom-up approach, such as hydrothermal and solvothermal synthesis.

4.1. Lithium Intercalation Methods

Chemical intercalation and exfoliation of bulk MoS₂ are the most traditional methods for the fabrication of metallic MoS₂.^[1,21,50,53,60,64–67] The mechanism for this method could be described as follows. In certain kinds of organic solvent, the bulk MoS₂ and a strong reducing reagent (*n*-butyllithium or LiBH₄) could form unstable lithium intercalated MoS₂ (Li_{*x*}MoS₂) by mixing them together to let lithium ions intercalate into. Afterward, the dispersed 2D MoS₂ could be facilely achieved by Li_{*x*}MoS₂ ultrasonication. These 2D flakes could be restacked by filtration and dispersion, and consequently result in the transformation of 2H phase to 1T metallic MoS₂ phase.^[50,53,68] Based on this, Eda et al.^[50] achieved the metallic MoS₂ by dissolving the natural MoS₂ together with butyllithium in hexane and allowed the reaction to occur for two days in

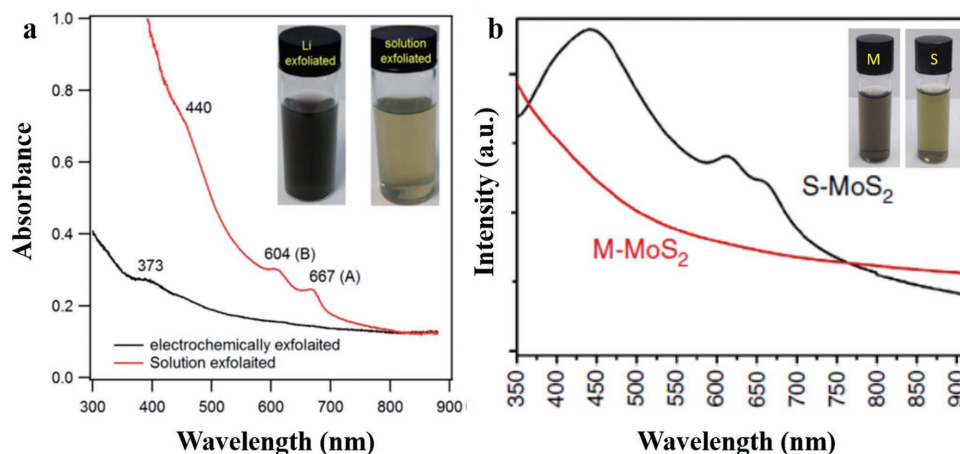


Figure 3. a) Optical absorption spectrum of MoS₂ dispersion in the mixture of water and isopropanol (1:1). Reproduced with permission.^[62] Copyright 2017, Royal Society of Chemistry. The red curve is the semiconducting phase. The black curve is the metallic phase. b) UV–vis spectrum of metallic MoS₂ (red curve) and semiconducting MoS₂ (black curve) dispersed in water. Reproduced with permission.^[28] Copyright 2016, Nature Publishing Group.

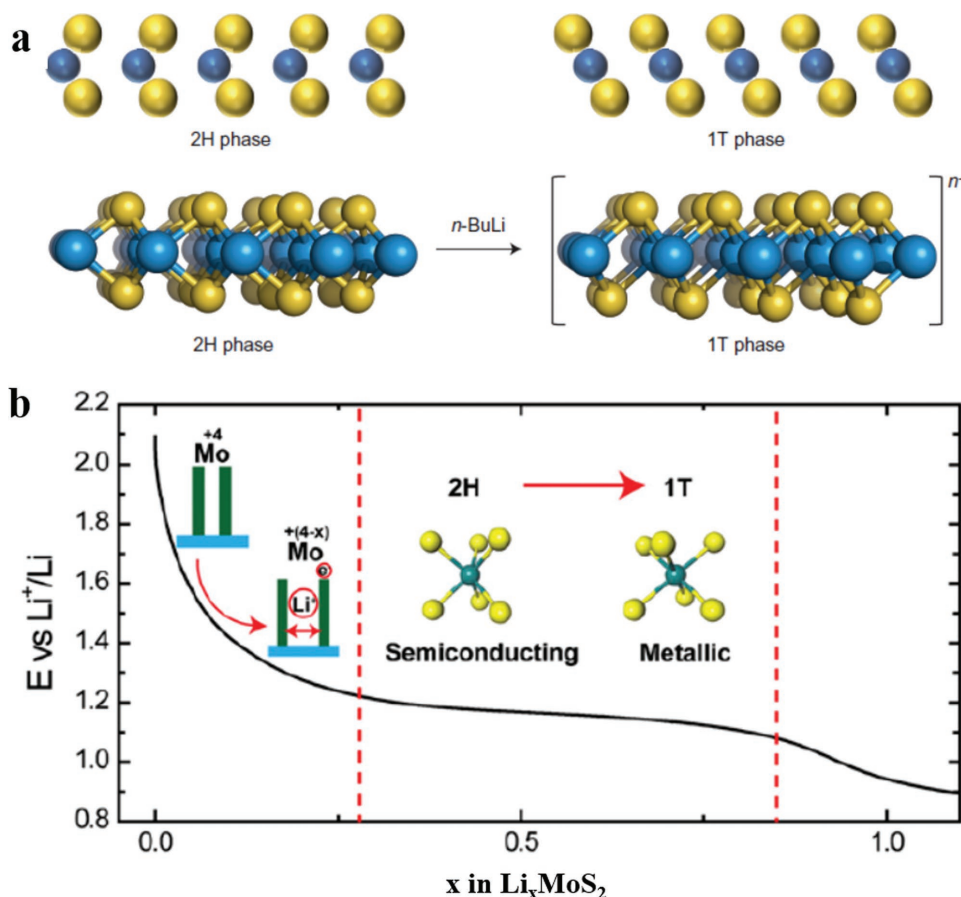


Figure 4. a) The atomic structure of semiconducting (2H) and metallic (1T) phases showing that the 2H phase can convert to 1T phase by butyllithium (BuLi) lithiation. Reproduced with permission.^[60] Copyright 2015, Nature Publishing Group. b) With lithium-ion intercalation, the semiconducting phase could also convert to metallic phase at certain voltage. Reproduced with permission.^[68] Copyright 2013, National Academy of Sciences.

an Argon environment. Acerce et al.^[37] successfully achieved the metallic MoS₂ monolayer nanosheets by exfoliating bulk MoS₂ with organolithium intercalation. Furthermore, Voiry et al.^[60] also successfully prepared single-layer metallic MoS₂ nanosheets with the similar method, by reacting *n*-butyl-lithium with MoS₂ crystal structure (Figure 4a).

Moreover, electrochemical Li-intercalation was also used to obtain the metallic MoS₂. Cui et al. assembled semiconducting MoS₂ film in the lithium-ion battery semicell as an anode and charged the cell up to a certain voltage to get the metallic phase MoS₂ (Figure 4b). Raman and XPS spectra were employed to verify the conversion of semiconducting MoS₂ into a metallic phase after charging to 1.1 V.^[69] One of the major advantages of this method is that the layer distance of MoS₂ can be precisely controlled by controlling the amount of intercalating lithium-ions into the MoS₂ layers at different voltages. However, this process is limited by the scalability, as it is not possible to produce a large quantity of metallic MoS₂ by this technique.

4.2. Solvothermal and Hydrothermal Method

Solvothermal and hydrothermal synthesis are typical bottom-up methods to fabricate metallic MoS₂. Wei et al. reported that by

using solvothermal method it is possible to acquire a composite of 2H MoS₂ and 1T MoS₂ by treating the 2H MoS₂ nanosheets in ethanol at 220 °C for 8 h.^[70] Recently, researchers find that N,N-dimethylfumarate (DMF) is an excellent candidate for a solvent as well as for accommodating guest molecules during the fabrication of expanded layer distance of metallic MoS₂ by solvothermal method. For example, Song et al.^[71] reported that the reaction of molybdate tetrahydrate and thiourea in the mixture of DMF and deionized water (1:4) by solvothermal method at 220 °C for 72 h (Figure 5a) can be used to prepare metallic MoS₂. The resultant MoS₂ owns an expanded layer distance of 0.98 nm. The same group proved that it is also possible to achieve the metallic MoS₂ in DMF without using any water by the reaction of molybdenum chloride and thioacetamide at 200 °C in autoclave.^[72] Pan et al.^[73] reported that metallic MoS₂ can also be fabricated by Na₂MoO₄·2H₂O and L-cysteine in a mixed solvent of DMF and water with a DMF to water ratio of 1.5:1 at 200 °C for 12 h (Figure 5b). The layer distance of the as-prepared metallic MoS₂ is around ≈0.90 nm that is much larger than the traditional layer distance of ≈0.62 nm.^[22] Song et al. proved that metallic MoS₂ could also be achieved by solvothermal method in the mixture of DMF and water of 1:50.^[74] Recently, our group published a fabrication technique of metallic MoS₂ by the reaction of molybdenum oxide and thioacetamide in ethanol (Figure 5c). The obtained metallic MoS₂

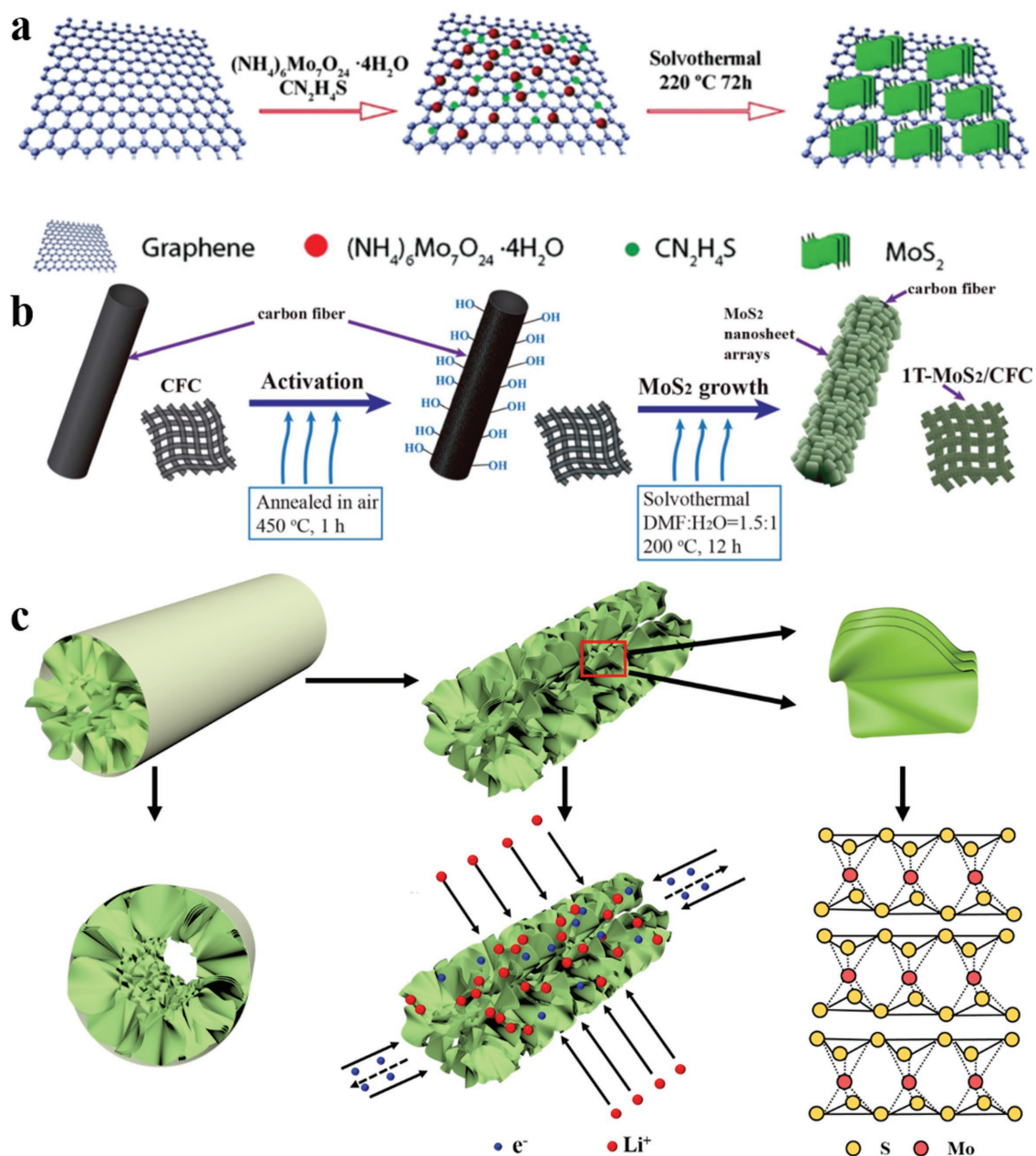
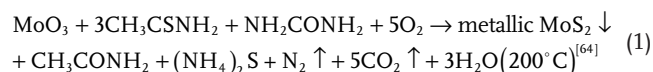


Figure 5. Solvothermal method. Schematic of the fabrication of metallic MoS₂ in a mixed solvent of DMF and water with a ratio of a) DMF:H₂O = 1:4; Reproduced with permission.^[70] Copyright 2017, Royal Society of Chemistry. b) DMF:H₂O = 1.5:1. Reproduced with permission.^[72] Copyright 2017, Royal Society of Chemistry. c) Schematic of the fabrication for metallic MoS₂ in ethanol. Reproduced with permission.^[30] Copyright 2018, Wiley-VCH.

can maintain its stability in air for more than 120 days and even after electrochemical charge/discharge.^[30]

Hydrothermal method is another strategy to fabricate metallic MoS₂. In 2015, Song et al.^[75] reported that with the reaction of NH₄⁺ rich ammonium molybdate tetrahydrate and thiourea in water, 2D metallic MoS₂ with a layer distance of ≈ 0.98 nm can be prepared. Chen and co-workers^[28] published another hydrothermal synthesis process of preparing metallic MoS₂ in water, which uses MoO₃ as the molybdenum precursor and template, and thioacetamide as the sulfur source and reduction agent. The dispersion of as-synthesized metallic MoS₂ nanosheets in water is stable for around 1 month and it

can retain its metallic phase for more than 90 days. Unfortunately, the repeatability of this process is still a problem due to some unknown factors. For the mechanism of the solvothermal or hydrothermal methods, different precursors have different reaction details, but the mechanism is similar. Take the metallic MoS₂ fabrication with octahedral MoO₃ as template as an example, the mechanism could be described as the following equation, and the result metallic MoS₂ could still maintain the octahedral structure of MoO₃



Since the metallic phase MoS₂ is metastable in nature, the fabrication approach turns to be much more important. The lithium ion intercalation method is the most popular method and has been proved to be an efficient way for the fabrication of metallic MoS₂. However, this method is complicated and takes days of time. Furthermore, the resulted product is usually a mixture with both metallic phase and semiconducting phase.^[36] With the presence of semiconducting phase, the metallic phase could be induced to semiconducting phase very quickly.^[28] Other approaches are also developed. For example, some paper reported that the metallic phase could be achieved from semiconducting phase under pressure as high as 35 GPa.^[39] But this method usually needs certain facility to realize, and not easy to be scalable. However, based on this strategy, scientists proved that by autoclave methods, under a certain pressure with proper chemical, the metallic phase MoS₂ could also be achieved. This method could be scalable and does not need specific facilities.^[30]

Herein, we also summarize several approaches to stabilize the metallic phase of MoS₂. Suenaga et al.^[76] reported that dopant atom, such as Re and Au, could help to stabilize the phase of metallic MoS₂. Bai et al.^[77] proved that the electrochemical lithiation process can also improve the stability of metallic MoS₂ phase. Song et al.^[71] claimed that when grown on graphene, the metallic MoS₂ could be efficiently confined, and prevented from aggregation. Zhu and co-workers^[30] reported a similar strategy to avoid MoS₂ aggregation, by designing a tube structure assembled with metallic MoS₂ nanosheets. This design will also help to avoid MoS₂ aggregation. Chen and co-workers^[28] also claimed that a much higher purity would also help a lot for metallic MoS₂ phase stability.

5. Characterizations

Metallic MoS₂ can be well distinguished from the semiconducting MoS₂ by their prominent differences in the morphologies and structures. In this section, we summarized the distinct morphological features of metallic MoS₂ observed in scanning electron microscopy (SEM), TEM, Raman spectra, X-ray diffraction pattern, and X-Ray photoelectron spectroscopy.

5.1. Microscope Morphology

The morphology of metallic MoS₂ directly fabricated by top-down or bottom-up method presents a typical 2D multilayer nanosheet structure. **Figure 6a,b** exhibits the SEM images of metallic MoS₂, which confirms the morphology as vertically aligned nanosheets, fabricated by autoclave. High resolution TEM (HRTEM) images (**Figure 6c,d**) show the layered structure of nanosheets, where the typical layer distance is around 0.65 nm. However, the layer distance can vary and be as large as ≈1 nm with the variation in reaction solvent such as water,^[22] ethanol, and DMF in autoclave.^[71] The Mo atom has a hexagonal arrangement with the distance ranging from 0.28 to 0.48 nm (**Figure 6e**).^[30] Selected area electron diffraction (SAED) pattern (**Figure 6f**) is another characterization method for MoS₂ based on HRTEM result. For metallic phase, the

diffraction rings are usually weak and hazy, reflecting the low degree of crystallization.^[30,35,73]

5.2. Spectroscopy

Raman spectroscopy, X-ray diffraction, and X-ray photoelectron spectroscopy are the typical spectroscopy characterization methods for the metallic MoS₂.

5.2.1. Raman Spectroscopy

In 1991, Sandoval et al.^[78] figured out the typical Raman peaks of metallic MoS₂ for the first time. As displayed in **Figure 7a**, the metallic MoS₂ has three peaks at 156, 226, and 333 cm⁻¹, marked as J₁, J₂, and J₃. The E_g mode of metallic with octahedral coordination of MoS₂ can be observed at 287 cm⁻¹. In contrast, the Raman peaks of semiconducting MoS₂ are at 372 (E¹_{2g}) and 400 cm⁻¹ (A_{1g}). Sandoval et al. also proved that the metallic phase was metastable in air by Raman measurement. As shown in **Figure 7a**, the A_{1g} peak of semiconducting MoS₂ intensifies after 12 days compared to a fresh sample. In addition, after 45 days the intensity of E¹_{2g} and A_{1g} peak increases drastically, whereas the intensity of J₁, J₂, and J₃ peaks reduces compared to a fresh sample. This phenomenon indicates a slow phase transformation of MoS₂ in air. Mallouk et al.^[79] confirmed that the peaks of E_g can switch between 284 and 307 cm⁻¹. Furthermore, other reports clarified that the J₁, J₂, and J₃ can also shift a little,^[65,66,80,81] which is probably due to the different layer distance. Generally, Raman spectra measurement is the most basic technique to identify the metallic phase of MoS₂. The easy operation procedure of Raman makes it the most convenient tool of identification. However, the stability of the metallic phase of MoS₂ can be affected by sonication, higher temperature, infrared laser, or even higher laser power of the Raman facility due to its metastable nature.^[28,79]

5.2.2. X-Ray Diffraction Pattern

XRD pattern further proves the differences between metallic MoS₂ and semiconducting MoS₂. As shown in **Figure 7b**, only one (002) peak appears before 14° for the semiconducting MoS₂, corresponding to the interplanar spacing of MoS₂ nanosheets. However, the metallic MoS₂ reveals a unique (001) peak around 7.3°, which evidences an additional layer separation of 0.55–0.60 nm during restacking.^[37] This specific peak was reported and explained as an expanded layer structure in 1987 by Frindt et al.^[82] followed by numerous recent researchers.^[28,35,38,71,73] The appearance of this (001) peak before 10° is the most conventional identification trait of metallic MoS₂ using XRD.

5.2.3. X-Ray Photoelectron Spectroscopy

XPS spectrum is another effective method to identify different phases of MoS₂. **Figure 7c,d** displays the differences in XPS

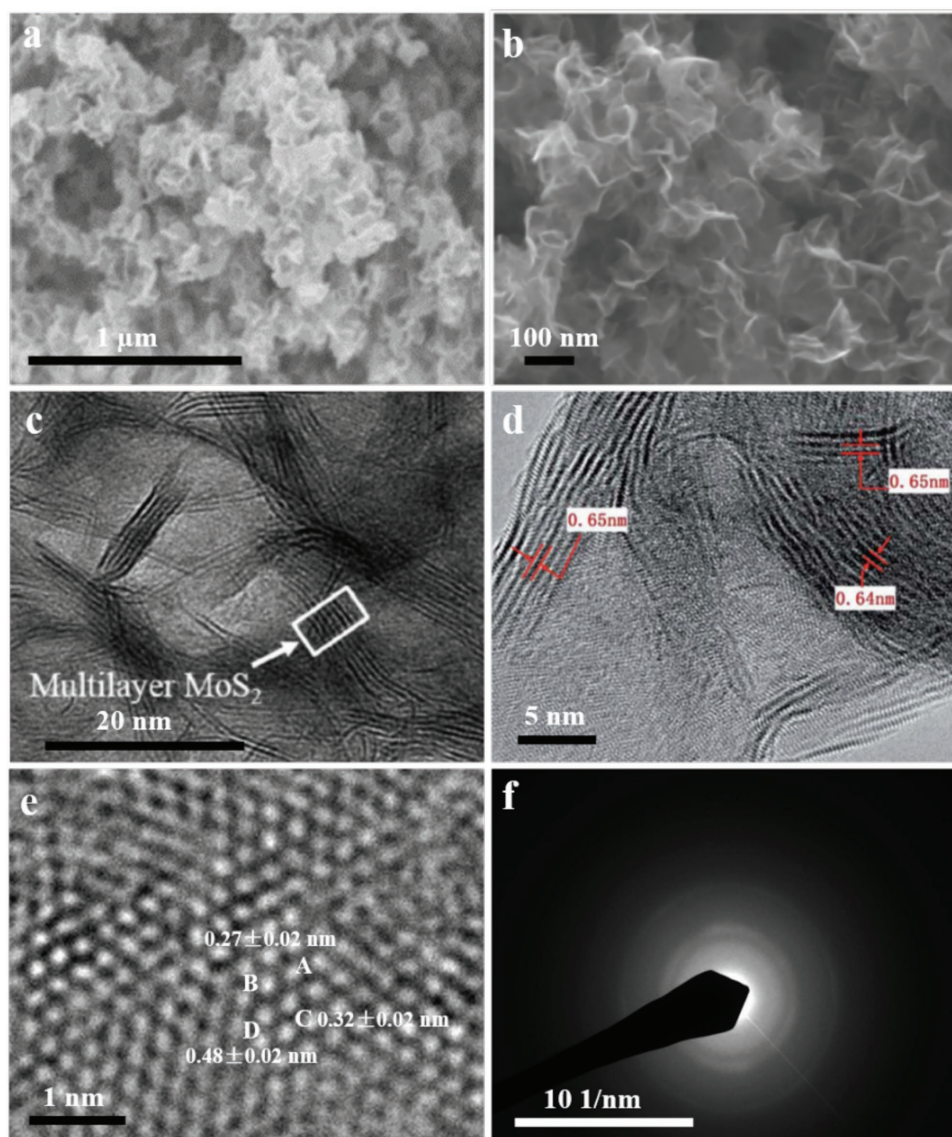


Figure 6. a,b) SEM images of metallic MoS₂. Reproduced with permission.^[22] Copyright 2017, American Chemical Society. Reproduced with permission.^[28] Copyright 2016, Nature Publishing Group. c,d) TEM images with the layer distance around 0.65 nm. Reproduced with permission.^[22] Copyright 2017, American Chemical Society. Reproduced with permission.^[35] Copyright 2017, Royal Society of Chemistry. e) Atom arrangement of metallic MoS₂ with the Mo–Mo distance. f) The selected area electron diffraction (SAED) pattern of metallic MoS₂. Reproduced with permission.^[30] Copyright 2018, Wiley-VCH.

profiles of semiconducting MoS₂ and metallic MoS₂, respectively.^[30] The XPS spectra of Mo element of metallic MoS₂ consists two signals; one at 228.7 eV corresponding to the 3d5/2 components and the other one at 231.8 eV regarding the 3d3/2 components Mo–S bonding. In contrast, the corresponding Mo signals of semiconducting MoS₂ are at 229.4 and 232.5 eV, which are ≈1 eV higher than the metallic MoS₂.^[50,83] Similarly, the S peaks of metallic MoS₂ are at around 161.6 eV for S 2P3/2 and 162.8 eV for 2P1/2 components. Also, the S signals of the semiconducting MoS₂ are ≈1 eV higher than the metallic MoS₂. XPS spectrum is also beneficial for verifying the Mo and S atom oxidation. The peaks at 236 and 169 eV related to the Mo⁶⁺ 3d5/2 and S oxidation will appear in case of any oxidation of Mo and S, respectively.^[50]

5.2.4. Synchrotron Radiation Based X-Ray Absorption Fine Structure (XAFS)

Synchrotron radiation based XAFS is another effective method to identify the metallic phase MoS₂. In detail, there are S K-edge spectra, Mo L3-edge X-ray absorption near edge structure (XANES) spectra, and Mo K-edge extended X-ray absorption fine structure (EXAFS) spectra for the metallic MoS₂.^[31] For S K-edge spectra (Figure 8a,b), there are characteristic peaks on 2471 and 2480 eV, and there is also a peak at 2469 eV, arising from the S 1s electron transfer. For 2H MoS₂, the characteristic peaks should be at 2471, 2479, 2482, and 2491 eV.^[70]

For the Mo L3-edge XANES (Figure 8c), the typical peak of 2H MoS₂ is at 2524 eV, and the intensity is much higher

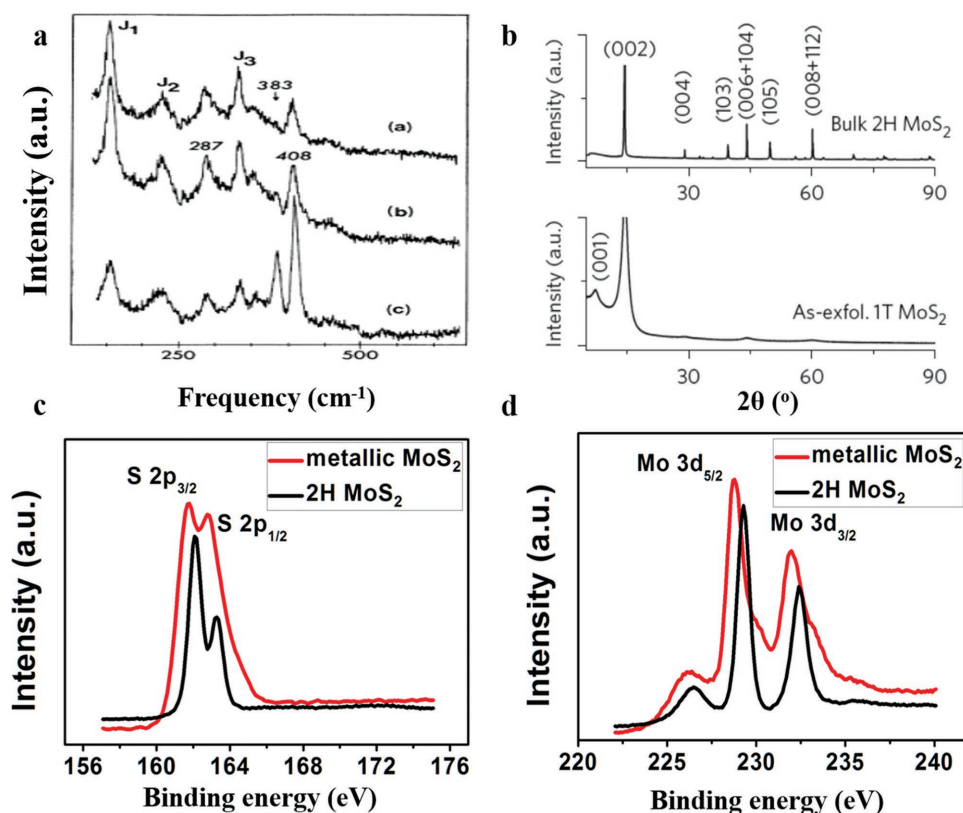


Figure 7. a) Raman patterns of metallic MoS₂ prepared by lithium intercalation and varying the storage time: a) fresh sample, b) sample after 12 days, and c) after 45 days. Reproduced with permission.^[77] Copyright 1991, American Physical Society. b) X-ray diffraction spectra of semiconducting MoS₂ and metallic MoS₂. Reproduced with permission.^[37] Copyright 2015, Nature Publishing Group. c,d) XPS spectra of c) Mo 3d and d) S 2p of the semiconducting MoS₂ and metallic MoS₂. Reproduced with permission.^[30] Copyright 2018, Wiley-VCH.

compared to metallic MoS₂.^[70] Furthermore, there is an extra shoulder peak appearing at 2522 eV for the metallic phase MoS₂, comparing to 2H MoS₂.^[31]

EXAFS spectra can help to investigate the Mo atoms bond lengths. For the metallic phase MoS₂, the Mo–Mo bonding EXAFS spectra (Figure 8d) would have two characteristic peaks at 1.9 and 2.5 Å, shows the metallic MoS₂ bond length should be at 1.9 and 2.5 Å. For 2H MoS₂, the peaks would be located at 1.9 and 2.9 Å.^[70]

6. Applications

Semiconducting MoS₂ is very promising anode material for lithium or sodium-ion batteries, owing to its high theoretical specific capacity (670 mA h g⁻¹) and low cost.^[84–88] Furthermore, the abundance of active sites and its layered structure also make it a good candidate for supercapacitors and HER. However, the low intrinsic conductivity and large bandgap (≈1.9 eV) significantly reduce the power density of the semiconducting MoS₂. Recently, metallic phase MoS₂ has emerged to be another potential material in the energy storage and conversion fields. Metallic MoS₂ electrode can exhibit an excellent electrochemical performance owing to its significantly high intrinsic conductivity. In recent years, several types of researches have been conducted to investigate the electrochemical performance

of MoS₂ for its application in batteries,^[30,71,73] supercapacitors,^[22,37] and HER.^[35,46,65]

6.1. Lithium-Ion Battery

Lithium-ion battery is the first possible application of metallic MoS₂ because of its high theoretical capacity and relatively mature research techniques. Song et al.^[71] demonstrated the excellent lithium-ion battery performance of metallic MoS₂ by designing a novel structure of interlayer expanded metallic MoS₂, vertically aligned on graphene. As shown in Figure 9a,b, the nanosheets are aligned on graphene, and the interlayer distance is around 0.98 nm, which is much larger than the standard layer distance of ≈0.62 nm. The material delivers an extremely high capacity of ≈1700 mA h g⁻¹ for the first cycle at a current density of 70 mA g⁻¹ with an initial coulombic efficiency of 70% (Figure 9d). Figure 9d also exhibits the rate performance of the electrode at current densities ranging from 70 to 3500 mA g⁻¹. The electrode provides a high capacity of 666 mA g⁻¹ even at a very high current density of 3500 mA g⁻¹, and it can deliver a reversible capacity of ≈1700 mA g⁻¹ when the current density is reduced back to the 70 mA g⁻¹.

Pan et al.^[73] fabricated metallic MoS₂ vertically aligned on carbon fiber cloth (Figure 9c) and demonstrated its

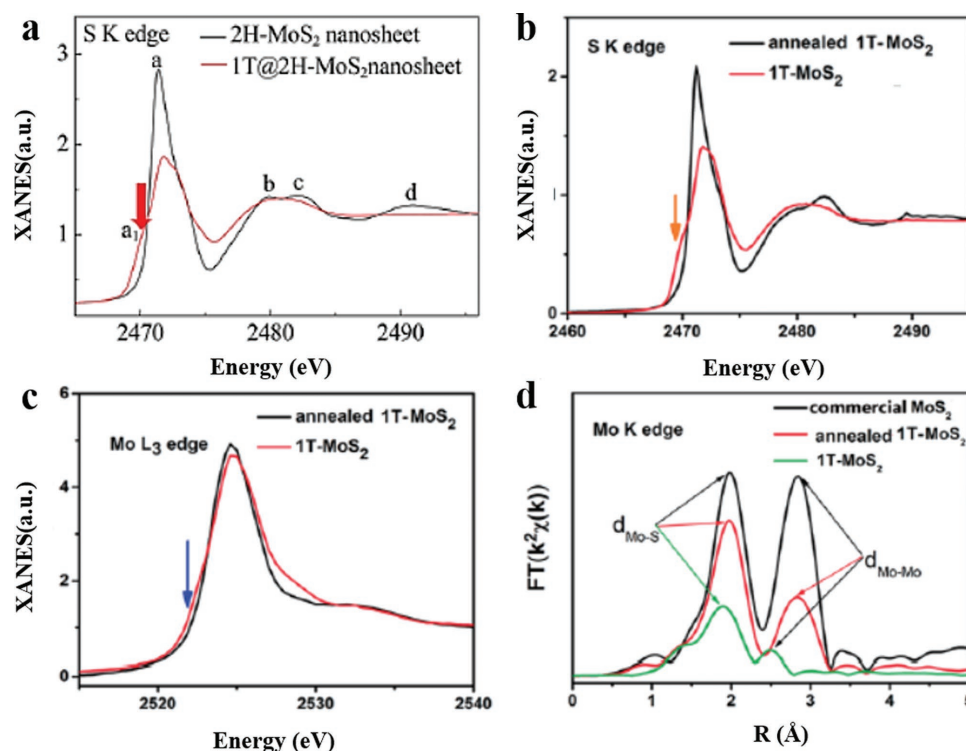


Figure 8. a) S K-edge spectra of 2H MoS₂. Reproduced with permission.^[69] Copyright 2015, American Chemical Society and b) 1T MoS₂. c) Mo L₃-edge XANES of 1T MoS₂. d) Mo–Mo bonding EXAFS spectra. Reproduced with permission.^[31] Copyright 2017, Royal Society of Chemistry.

electrochemical performance in lithium-ion batteries. As shown in Figure 9e, the composite anodes of metallic MoS₂ and carbon cloth provide extremely high capacities of 2210 and 1789 mA h g⁻¹ at a current density of 0.1 A g⁻¹ with an initial coulombic efficiency of 81%. Furthermore, the anode can retain its capacity of 800 mA h g⁻¹ at a high current density of 2 A g⁻¹. It also maintains 77% of its initial capacity after returning to a lower current density of 0.1 A g⁻¹, which represents the decent rate performance of the composite anode. In addition, at a high current density of 1 A g⁻¹, the anode delivers a high reversible capacity of 853 mA h g⁻¹ for 140 cycles (Figure 9f).

Although the rate performance, reversible capacity, and cycling stability are not comparable to hybrid semiconducting MoS₂/ carbon materials; these researches establish the possibility of metallic MoS₂ for battery applications. However, both of these works employed high conductive carbon sources (carbon cloth or graphene) as host to improve the conductivity of the metallic MoS₂ electrode. Therefore, suppress the most advantageous aspect, high intrinsic conductivity of metallic MoS₂.

Recently, our group designed novel carbon-free and porous nanotubes, assembled with 2D pure metallic MoS₂ nanosheets (Figure 10a).^[30] The nanotube structure can effectively reduce the risk of restacking the nanosheets that subsequently enhances the stability of the metallic phase and improves the ion transportation capability. The structure can retain its metallic phase for at least 120 days in air, as shown in Figure 10b. Figure 10c shows the difference between the cyclic voltammetry (CV) curves of metallic phase and 2H phase of the MoS₂. Compared to the 2H phase, the pure metallic phase does not own peaks ≈1 V, which are the typical peaks for the transformation of 2H phase to 1T

phase, during the lithium intercalation. In addition, an apparent anodic peak ≈1.5 V, which is the most distinct anodic peak, appears for the metallic phase of MoS₂ in lithium-ion batteries. To further confirm the advantages of pure metallic MoS₂, the battery was cycled at the current density of 5 A g⁻¹ (Figure 10d). The metallic MoS₂ nanotubes could deliver a reversible specific capacity of ≈935 mA h g⁻¹ for 200 cycles at the current density of 5 A g⁻¹. The capacity can further increase to ≈1150 mA h g⁻¹ after 350 cycles due to the reversible formation of organic polymeric/gel-like layer through electrolyte decomposition. Furthermore, with the high intrinsic conductivity, the anode exhibits outstanding rate performances at the current density ranging from 0.2 to 20 A g⁻¹. As shown in Figure 10e, even at extremely high current density of 20 A g⁻¹, the metallic nanotubes still maintain a reversible capacity of 589 mA g⁻¹, which is much higher than the low conductivity semiconducting MoS₂ (≈150 mA h g⁻¹). Figure 10f shows the Raman spectra before and after cycling. Even after cycling for 350 times as an anode in a lithium-ion battery, the MoS₂ nanotubes retain the metallic phase that again proves the advantage of the nanotube structure on stabilizing the metallic phase. Overall, this work highlights the superior conductivity of metallic MoS₂ and demonstrates the benefits of using metallic MoS₂ without any conductive additives in batteries specifically at high current densities.

6.2. Sodium-Ion Battery

Sodium-ion batteries are another promising option for energy storage due to the low cost, low toxicity, readily accessible, and

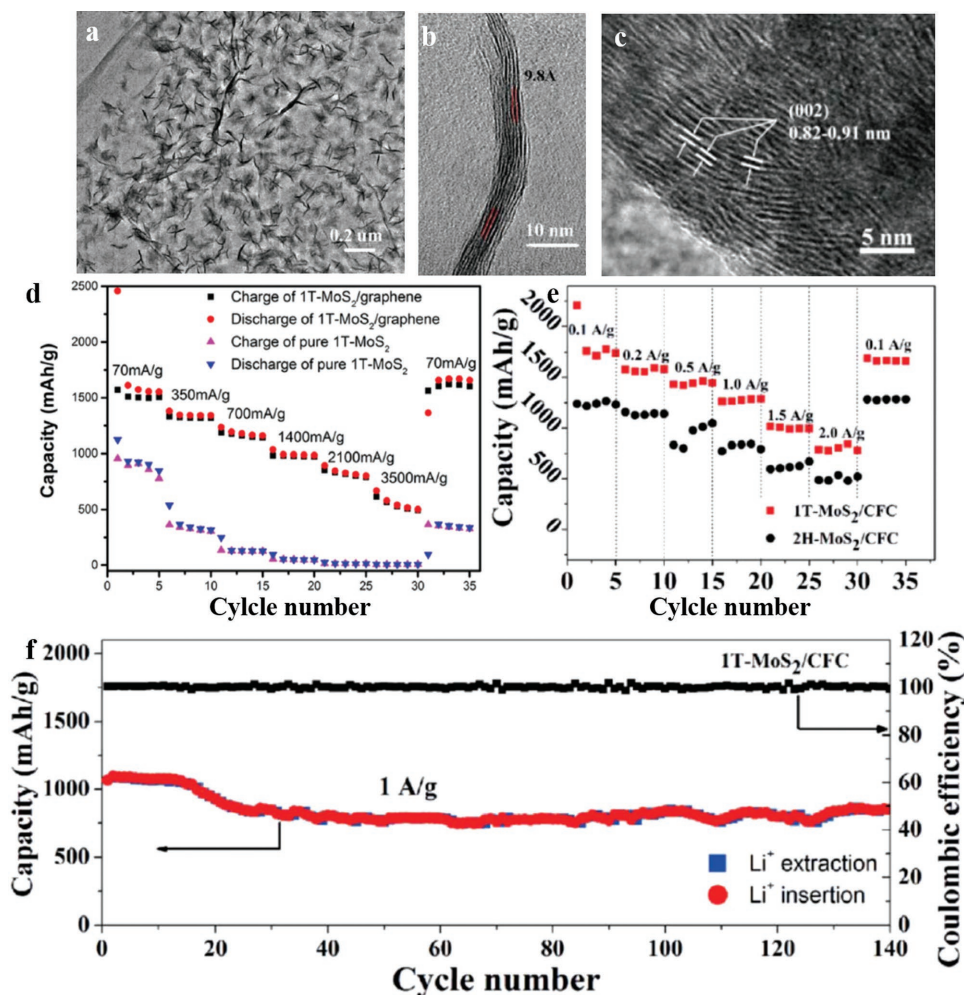


Figure 9. a) TEM image of MoS₂ on graphene.^[71] b) HRTEM image of metallic MoS₂ to show the interlayer distance.^[71,73] c) HRTEM image of MoS₂ on carbon fiber cloth.^[71,73] d) Rate performance at current densities ranging from 0.1 to 2 A g⁻¹ for metallic MoS₂ on graphene.^[71,73] e) Rate performance at current densities ranging from 0.1 to 2 A g⁻¹ for metallic MoS₂ on carbon fiber cloth.^[71,73] f) Cycling stability and coulombic efficiency of metallic MoS₂ and carbon cloth at 1 A g⁻¹. Reproduced with permission.^[70] Copyright 2017, Royal Society of Chemistry. Reproduced with permission.^[72] Copyright 2017, Royal Society of Chemistry.

earth-abundance of sodium. However, the radius of sodium ion (99 pm) is much larger than lithium ion (59 pm), which influences the capacity, stability, and overall battery performance.^[29]

Recently, our group reported a new, effective method for direct synthesis of metallic 1T MoS₂ on 3D hollow graphene foam that results in a freestanding and lightweight nanostructure with the high mass loading of active material. We demonstrate for the first time the use of metallic 1T MoS₂ as an intercalation anode for sodium ion batteries.^[29] Figure 11a shows the schematic of the as-designed hollow structure and the vertically grown metallic MoS₂ on both the internal and external walls of each graphene tube to form a freestanding MoS₂–graphene–MoS₂ sandwich electrode. The porous, hollow structure of the electrode allows maximum electrolyte accessibility and the graphene backbone provides excellent electrical conductivity. The high conductivity of the metallic MoS₂/graphene structure facilitates a high capacity of 175 mA h g⁻¹ at a high current density of ≈3 C (2 A g⁻¹) and the structure recovers a capacity of ≈313 mA h g⁻¹ after the current density is

reduced back to 50 mA g⁻¹, as shown in Figure 11b. The anode also delivers a high capacity of 630 mA h g⁻¹ while cycling at a current density of 50 mA g⁻¹ and stabilizes at around 313 mA h g⁻¹ for 200 cycles, which displays an excellent cycling stability (Figure 11c).

6.3. Supercapacitors

Supercapacitors, one of the most widely used energy storage devices, have received significant attention in recent years.^[89] As a typical 2D TMD, MoS₂ has already been studied as electrode in supercapacitors. The layered structure provides large surface area, which leads to more double-layers and pseudocapacitors stored in per unit voltage, and the Mo ions possess a range of oxidation state from +2 to +6 which causes more pseudocapacitor behavior and hence results in higher specific capacity.^[90–92] However, the semiconducting 2H phase of MoS₂ is not the best choice for supercapacitors due to its intrinsic semi conductivity.

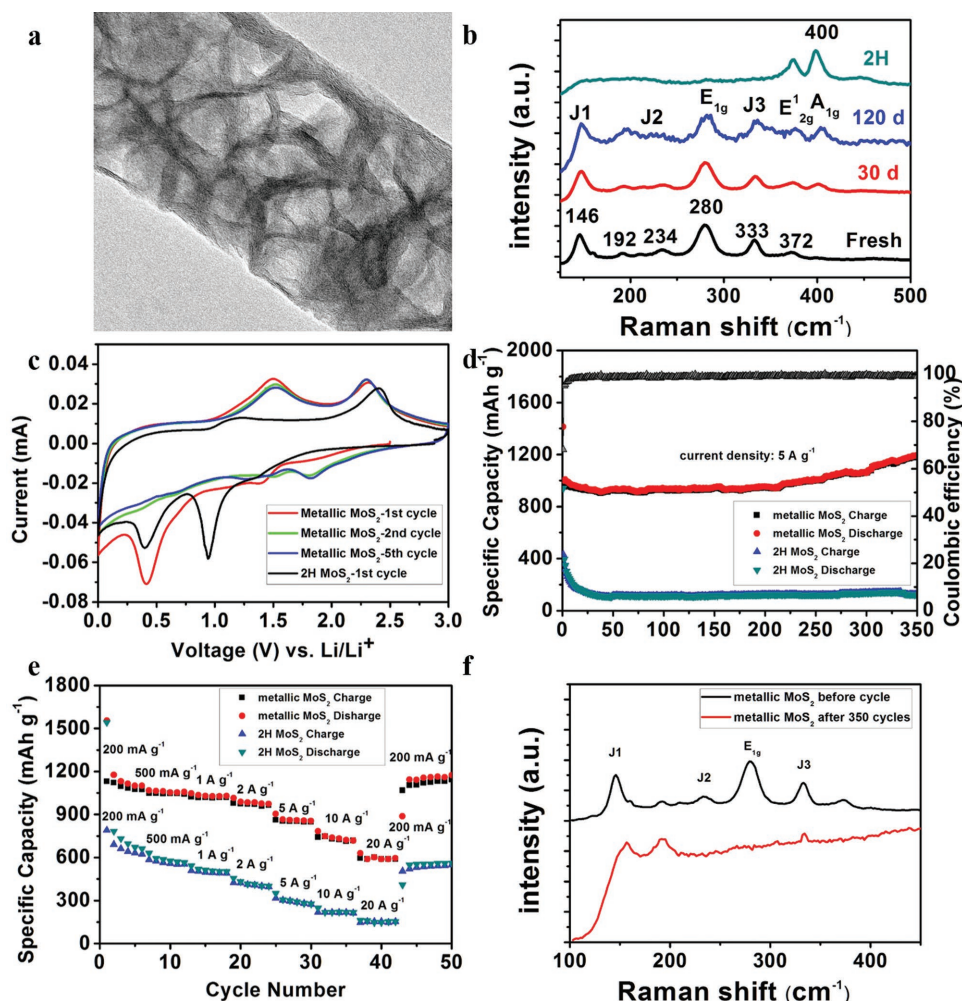


Figure 10. a) HRTEM image of the metallic MoS₂ nanotube showing the porous and layered structure. b) Raman patterns of the metallic MoS₂ nanotube after storing it in air for several days and corresponding Raman pattern of 2H MoS₂ nanosheets. c) CV curves of metallic MoS₂ for different cycles and the 1st cycle of 2H MoS₂ in lithium-ion batteries. d) Cycling stability and coulombic efficiency of metallic MoS₂ and semiconducting MoS₂ at 5 A g⁻¹. e) Rate performance of metallic and 2H MoS₂ at different current densities ranging from 0.2 to 20 A g⁻¹. f) Raman spectra of metallic MoS₂ before and after 350 cycles. Reproduced with permission.^[30] Copyright 2018, Wiley-VCH.

Therefore, the metallic MoS₂ has gained large attention due to its much higher conductivity and activity.^[93–95]

Our group reported a multilayer metallic MoS₂–H₂O system with nanochannels, where the bilayer water molecules are sandwiched between the single layers of metallic MoS₂ through a hydrothermal process using water as solvent. The work also includes an investigation of the electrochemical performance of pure metallic phase of MoS₂ as a supercapacitor electrode.^[22] In **Figure 12a**, the schematic illustrates the multilayer structure of the metallic MoS₂–H₂O system as an electrode in a supercapacitor. This structure of the electrode is beneficial, as it provides a pathway for the ions and electrons transportation along the nanochannels between the MoS₂ layers through the inner layer of the water molecule and the conducting metallic MoS₂ sheets, respectively. **Figure 12b** shows the XRD pattern of the metallic MoS₂–H₂O system that verifies the presence of water monolayer and the special structure.^[28] The rectangular shape of the CV curves in different electrolytes indicates the

good capacitive behavior of the electrodes (**Figure 12c**). The galvanostatic charge/discharge profiles (**Figure 12d**) of metallic MoS₂–H₂O electrode performed exhibit the best capacitive behavior in the Li₂SO₄ electrolyte, as it is much easier for lithium ions to enter the nanochannels created by the expanded interspace with water layers due to the larger layer distance and the higher hydrophilicity. In **Figure 12e**, the current density shows a linear relationship with the scan rate, which further confirms the excellent conductivity and capacitive performance of the metallic MoS₂–H₂O. Note that there is no any conductive additive existed in the electrode. When tested in symmetric MoS₂ supercapacitor at a high current density of 5 A g⁻¹, a specific capacitance of 150 F g⁻¹ was achieved. It also retained 88% of its original capacity even after 10 000 cycles, as shown in **Figure 12f**. Therefore, it can be concluded that the excellent electrochemical performance is the result of the high electric conductivity of the metallic 1T MoS₂ and the expanded interspaces with water molecules between the layers.

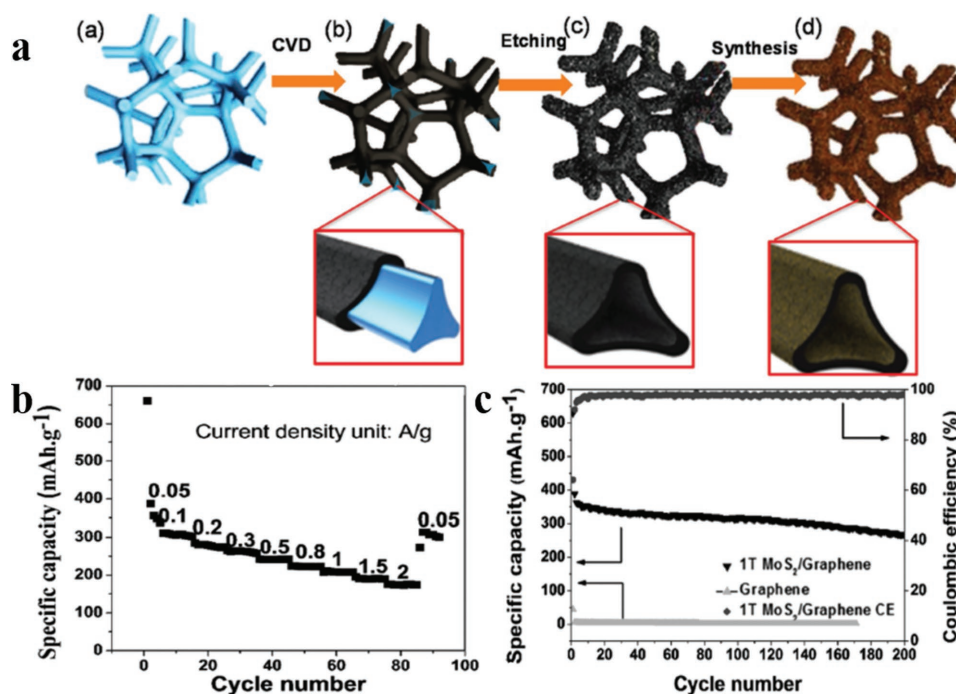


Figure 11. a) Schematic illustration of the 3D metallic MoS₂-graphene-MoS₂ structure preparation. b) Rate performance of the metallic MoS₂-graphene electrode at different current densities ranging from 0.05 to 2 A g⁻¹. c) Cycling stability and coulombic efficiency at a current density of 50 mA g⁻¹. Reproduced with permission.^[29] Copyright 2017, Wiley-VCH.

In parallel with the bottom-up method, several other approaches have also been made to fabricate metallic MoS₂. Chhowalla and co-workers^[37] reported a top-down strategy using organolithium chemistry to exfoliate the bulk MoS₂ powders into monolayer nanosheets with a combination of ≈70% 1T phase and 100% monolayered MoS₂, which were further restacked to a flexible film using a simple filtration method. According to the XRD spectra and the schematic of the metallic MoS₂ with/without ions intercalation, as shown in Figure 13a,b, the restacked MoS₂ film has an enlarged interspace of 6.15 Å that was expanded to 9.85, 12.78, 12.24, and 10.98 Å after K⁺, Li⁺, Na⁺, and TEA⁺ ions intercalation, respectively. The volumetric capacitances in various aqueous electrolytes depend on the scan rates and maintained between 400 and 650 F cm⁻³ in the 20 mV s⁻¹, which is much higher than the 2H MoS₂ (Figure 13c). In the galvanostatic charge/discharge measurements at a current density of 2 A g⁻¹, the restacked MoS₂ film offers a high capacitance of ≈370 F g⁻¹ even after 5000 cycles. It also retains greater than 93% of its initial capacity in neutral electrolytes and greater than 97% in acidic electrolytes. In addition, the electrochemical storage behavior of the restacked MoS₂ film in a nonaqueous electrolyte (TEABF₄) was also investigated using a two-electrode system where the electrode delivers a high capacitance of ≈180 F cm⁻³ and retains more than 90% of its initial capacity after 5000 cycles at a current density of 1 A g⁻¹ (Figure 13d). To sum up, compared with 2H phase, metallic MoS₂ is more hydrophilic which leads to fast ion diffusion. Therefore, considering the higher conductivity, metallic MoS₂ often behaves better performance than semiconductor phase at higher current density and scan rate when used as supercapacitor electrode.^[22,37]

6.4. Hydrogen Evolution Reaction (HER)

Green energy conversion such as using catalysis hydrogen evolution as a green source of energy has attracted much interest as a promising replacement for fossil fuels.^[96] Efficient electrocatalysts should be used in order to obtain efficient and sustainable HER.^[97-99] In particular, these electrocatalysts must satisfy two basic characteristics. First, the catalyst must be highly active toward HER, i.e., it should be capable of producing a high amount of hydrogen gas at a minimum overpotential. Second, it should be chemically and physically stable enough to maintain its efficiency over time.^[100] Platinum (Pt) and other noble metals have been commonly known as the most efficient electrocatalysts for HER. However, their high cost and low abundance restricted their usage on a large scale for commercial applications. To overcome this limitation, a lot of researches have been focused on finding other alternative electrocatalysts with low cost and abundance for HER. These include metal oxides,^[101,102] enzymes,^[103] bioinspired molecular materials,^[104,105] and very recently TMDs.^[98,99,106-109] Metallic 1T MoS₂, as one of TMDs family, has shown very promising catalytic activity recently for HER. This is mainly due to the increased number of electrocatalytic active edge sites of the 1T metallic phase and the increased structural defects compared to its 2H semiconducting phase counterpart. In this section, we are reporting the recent progress in the catalytic performance of 1T MoS₂ for HER in both electrocatalysis and photocatalysis applications and the techniques that can be further modified to enhance its catalytic activity.

Experimentally, it has been proven that chemical exfoliation of 2H MoS₂ semiconducting phase to metallic 1T MoS₂ nanosheets dramatically enhances HER catalysis.^[65] As shown

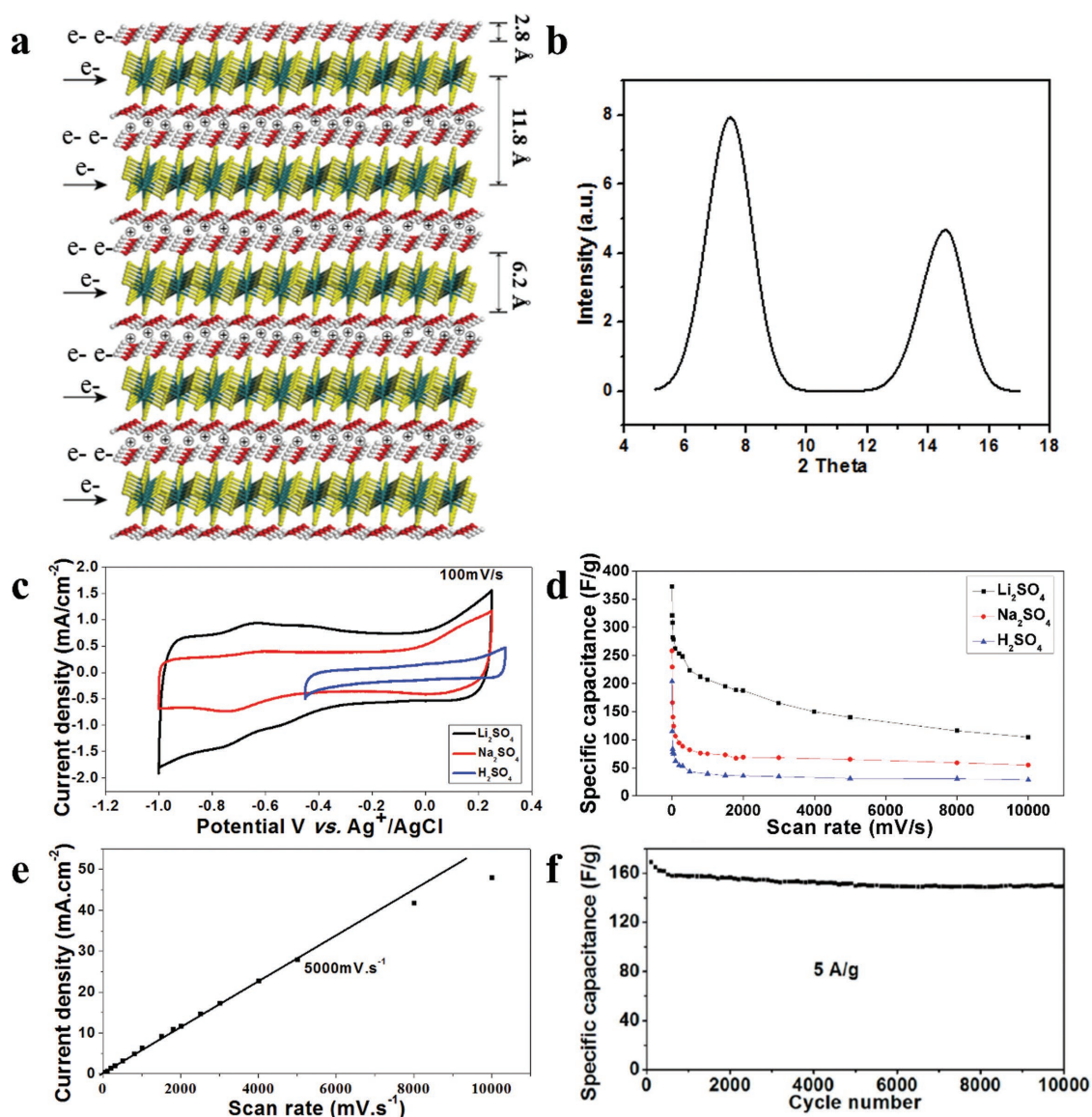


Figure 12. a) Schematic illustration of the multilayer metallic $\text{MoS}_2\text{-H}_2\text{O}$ based symmetric supercapacitor. b) XRD of metallic $\text{MoS}_2\text{-H}_2\text{O}$ in the standard three electrodes system. c) CV curves for three kinds of electrolytes at the same scan rate of 100 mV s^{-1} . d) Galvanostatic charge/discharge performance under different scan rates in three kinds of electrolytes. e) Plot of current density versus scan rates showing a linear relationship. f) The long-term cycling of the symmetric electrochemical supercapacitor. Reproduced with permission.^[22] Copyright 2017, American Chemical Society.

in **Figure 14a**, the polarization curve of the as-grown 2H MoS_2 shows an onset overpotential at -200 mV (vs RHE). However, significant H_2 evolution at the current density of 10 mA cm^{-2} was only achieved at -320 mV . In contrast, 1T MoS_2 showed dramatically enhanced performance, where significant H_2 evolution (at $J = 10\text{ mA cm}^{-2}$) was shifted to much lower overpotential of -195 mV versus RHE. The corrected raw data for IR losses revealed even more promising performance with -187 mV versus RHE at $J = 10\text{ mA cm}^{-2}$. Moreover, the Tafel plot in **Figure 14b** further revealed the enhancement with 54 and 43 mV per decade for the raw and IR corrected data of the exfoliated 1T MoS_2 nanosheets, respectively. Whereas the as-grown nanostructures showed higher slope of 117 and 110 mV per decade for the raw and IR corrected data, respectively. This is due to the favorable kinetics, enhanced conductivity, and the

increasing number of active sites of exfoliated 1T MoS_2 . On the other hand, Gao et al.^[46] further proved theoretically, using first-principles calculations, that the 1T MoS_2 phase transition from its 2H MoS_2 phase can be stabilized via charge injection. Furthermore, by taking this injection into account, the metallic 1T' MoS_2 would show superior catalytic activity compared to semiconducting 2H MoS_2 . As shown in **Figure 14c**, the phase transition from 2H MoS_2 to 1T MoS_2 involves the movement of one S atom from one pyramidal position to the other pyramidal position of the unit cell. **Figure 14d** shows that the pathway relative energy for this phase transition decreased from 0.8 and 0.31 eV in the neutral and $1e^-$ charge state to -0.05 , -0.1 , and -0.3 eV in the charge states of $2e^-$, $3e^-$, and $4e^-$, respectively. This confirms that the charge injection can stabilize the 1T MoS_2 phase. Moreover, the phase transition energy barrier is

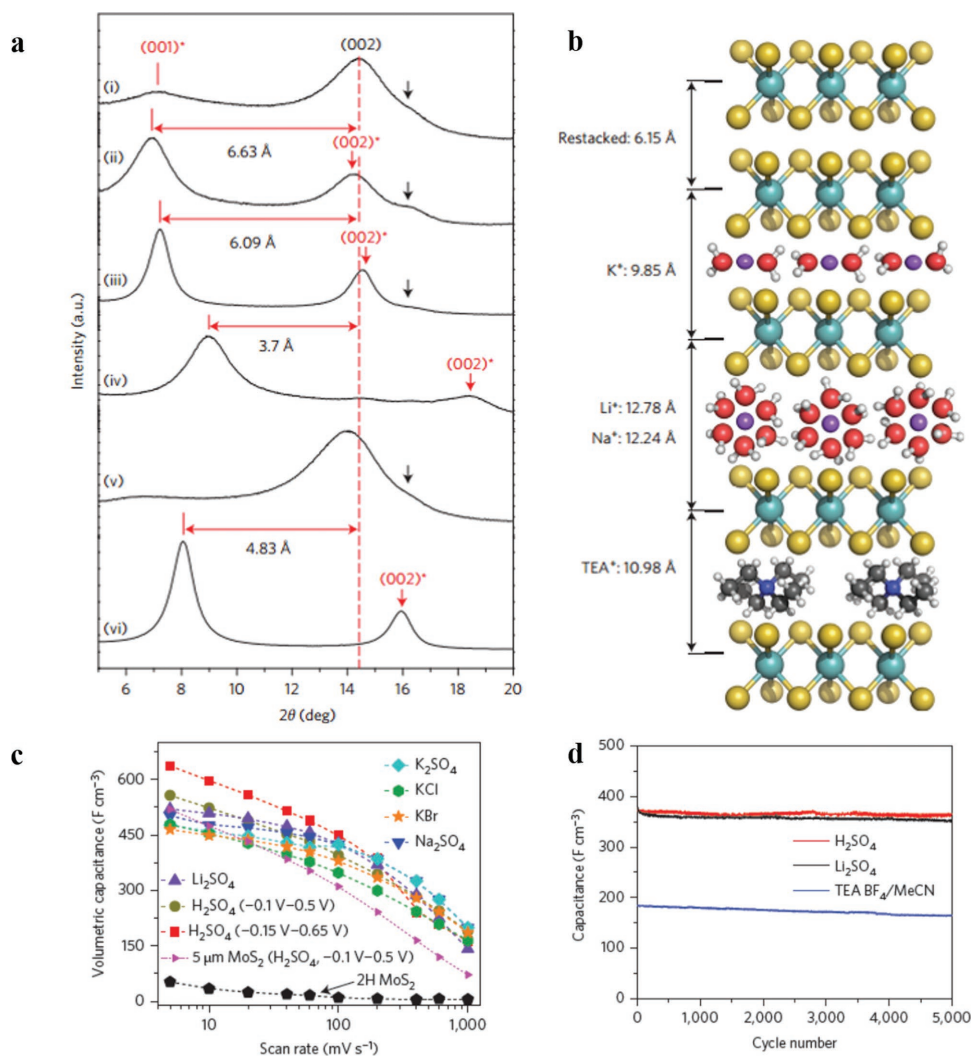


Figure 13. a) XRD spectra of (i) the 1T-MoS₂ nanosheets and cycled MoS₂ film in various sulphate-based electrolytes: (ii) Li₂SO₄, (iii) Na₂SO₄, (iv) K₂SO₄, (v) H₂SO₄, and (vi) TEA BF₄/MeCN organic electrolyte. b) Schematics of the restacked 1T MoS₂ that deintercalated and intercalated with different cations. c) Evolution of the volumetric capacitance with scan rates for different electrolytes and 1 and 5 μm thick films. The concentration of the cations in the electrolyte solution was fixed at 1 M; d) Capacity retention after 5000 cycles in 0.5 M Li₂SO₄, H₂SO₄, and 1 M TEA BF₄ in acetonitrile. Reproduced with permission.^[37] Copyright 2015, Nature Publishing Group.

decreased from 1.59 eV in the neutral structure to 1.11, 0.71, 0.54, and 0.27 eV in charge states of 1e⁻, 2e⁻, 3e⁻, and 4e⁻, respectively. These studies directed the attention of researchers to further investigate the catalytic activity of 1T MoS₂ metallic phase for H₂ evolution. This can solve the limitation of using Pt and other low abundance noble metals on a large scale.

Chua et al.^[110] established a study to evaluate the efficiencies of the bottom-up (hydrothermal reaction) and top-down (chemical exfoliation) approaches in producing metallic 1T MoS₂. They found that metallic 1T MoS₂ phase produced through the bottom-up approach contains a higher proportion of metallic 1T MoS₂ and demonstrates excellent electrochemical and electrical properties. Chen and co-workers^[28] synthesized highly pure and stable metallic MoS₂ nanosheets using controllable hydrothermal solution method. The measured HER activity was very promising compared to the semiconducting MoS₂ counterparts with a low potential of 175 mV versus RHE at

a current density of 10 mA cm⁻² and a Tafel slope of 41 mV per decade for 1T MoS₂. Recently, Qin et al.^[72] revealed that metallic 1T MoS₂ grown on single-walled nanotubes can reduce the absorption energy of H⁺ atoms via electron doping, which renders the structure superior electrocatalytic performance with outstanding HER activity of ≈40 mV onset overpotential and a low Tafel slope of 36 mV per decade. This methodology can be further applied to improve the conductivity of other TMDs materials as well. On the other hand, Wang et al.^[111] rooted metallic 1T MoS₂, prepared by hydrothermal exfoliation, into 1D TiO₂ nanofibers, upon investigating its catalytic activity for HER, they found that the metallic 1T MoS₂ phase serves as metastable phase during HERs, and can be irreversibly transformed into more active metallic 1T' phase as true active sites, which leads to higher HER activities. Zhao et al.^[112] prepared MoS₂ nanoflowers with predominant 1T MoS₂ phase doped with FeS₂, after investigating its catalytic performance

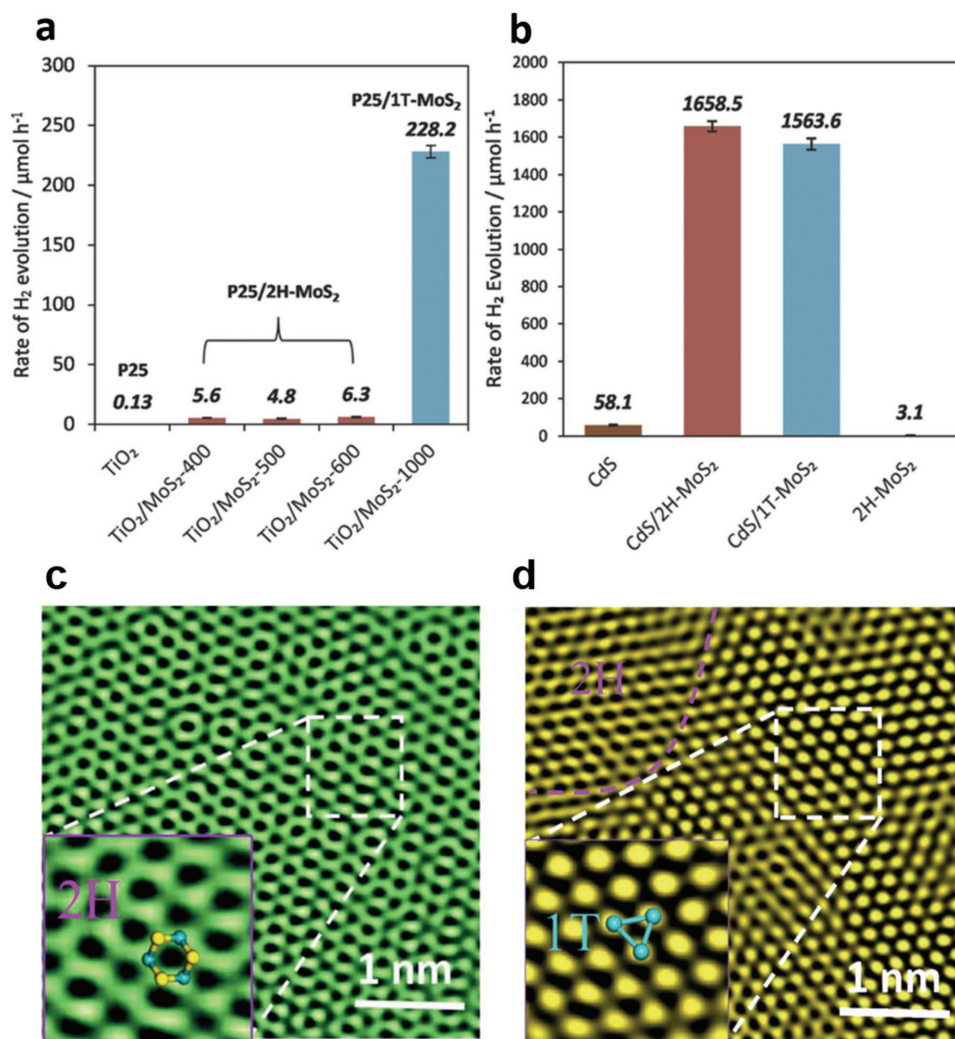


Figure 15. a) H₂ evolution photocatalytic activity of 1T and 2H MoS₂ over TiO₂-P25. b) H₂ evolution photocatalytic activity of 1T (MoS₂-1000) and 2H phases MoS₂ (MoS₂-400) over commercial CdS. Reproduced with permission.^[114] Copyright 2016, Wiley-VCH. HRTEM images of the MoS₂ in TiO₂@MoS₂ c) before and d) after exfoliation (insets show the 2H and 1T phases in (c) and (d), respectively). Reproduced with permission.^[110] Copyright 2017, Wiley-VCH.

Maitra et al.^[113] revealed that single layer metallic 1T MoS₂ with heavily nitrogenated reduced graphene shows outstanding performance in H₂ production under visible light. The metallic 1T MoS₂ evolved 30 mmol g⁻¹ h⁻¹, which was 600 times higher than its 2H MoS₂ counterpart. Also, Qin et al.^[114] reported the fabrication of stable metallic 1T MoS₂ slabs grown on CdS nanorods using solvothermal approach. The metallic 1T MoS₂@CdS heterostructure significantly improves the photocatalytic activity for CdS samples; they related this improvement to the intimate contact at the interface and the metallic conductivity of metallic 1T MoS₂, which resulted in enhanced charge separation and fast kinetics for electrons transfer to reduce H₂O adsorbed on metallic 1T MoS₂. On the other hand, Chang et al.^[115] compared the photocatalytic hydrogen evolution activity of 2H and 1T MoS₂, by combining them with P25-TiO₂ and CdS photoharvesters to create nanocomposite TiO₂/MoS₂ and CdS/MoS₂, as shown in **Figure 15a**, Bare P25-TiO₂ cannot offer active sites for catalytic H₂ evolution because of its high

crystallinity, with H₂ evolution rate of 0.13 $\mu\text{mol h}^{-1}$. Moreover, semiconducting 2H MoS₂ did not show obvious improvement even with different exfoliation degrees. In contrast, TiO₂/MoS₂ nanocomposite showed drastic enhancement for H₂ evolution with 228.2 $\mu\text{mol h}^{-1}$, corresponding to a quantum yield of 14.5% under 365 nm irradiation. **Figure 15b** shows the performance with CdS as photoharvester. Similar to that obtained with bare TiO₂, CdS showed poor photocatalytic activity for H₂ evolution, 228.2 $\mu\text{mol h}^{-1}$. However, in this case, both metallic 1T MoS₂/CdS and metallic 1T MoS₂/CdS showed promising performance with 1563.6 and 1658.5 $\mu\text{mol h}^{-1}$ H₂ evolution. The authors related the enhancement in the 2H MoS₂ case to its smaller particle size, which can be easily adsorbed to the CdS surface, providing a better contact for the transport of the photoexcited electrons. Wang et al.^[111] prepared highly stable metallic 1T MoS₂ that is vertically rooted over TiO₂ nanofiber. After investigating their photocatalytic activity before and after exfoliation, the exfoliated TiO₂@MoS₂ showed a superlinear

increase over time, giving a better photocatalytic performance. Figure 15c,d shows the HRTEM images for the $\text{TiO}_2@\text{MoS}_2$ before and after exfoliation, respectively. The results confirm the presence of nearly pure 2H MoS_2 in $\text{TiO}_2@\text{MoS}_2$ before exfoliation, whereas the metallic 1T phase is dominant after exfoliation and constitutes $\approx 60\%$ of the MoS_2 structure, this interprets the better performance detected after exfoliation.

Yue et al.^[116] prepared cracked monolayer metallic 1T MoS_2 with a porous structure, using ultrasonication of enhanced lithium intercalated MoS_2 nanosheets. The cracked metallic 1T MoS_2 structure exhibited excellent hydrogen evolution performance with a low overpotential (156 mV vs. RHE) at 10 mA cm^{-2} , the Tafel slope was only 42.7 mV per decade. This is a result of the large proportion of active sites introduced via the porosity within the monolayer nanosheets. Recently, Li et al.^[117] succeeded to synthesize hybrid photocatalysts for hydrogen evolution by integrating metallic 1T MoS_2 nanosheets, and inorganic-ligand stabilized CdSe/ZnS quantum dots via self-assembly approach. The hybrid structure can produce H_2 gas with a rate of $\approx 155 \pm 3.5 \mu\text{mol h}^{-1} \text{mg}^{-1}$ under visible-light ($\lambda = 410 \text{ nm}$). These results represent promising performance for metallic 1T MoS_2 as a photocatalyst for solar H_2 evolution. It should be mentioned that, unlike the well proven electrocatalytic H_2 evolution, metallic 1T MoS_2 H_2 evolution photocatalytic activity is still in its infancy, and further research is still needed to investigate this field.

This recently achieved results for metallic 1T MoS_2 shed light on the power of 1T MoS_2 as a promising HER catalyst. However, further study is still needed to enhance its stability and to further improve their catalytic performance to be a suitable replacement for Pt and other noble metals in the near future for H_2 evolution.

7. Conclusions and Perspectives

In summary, we reviewed the structure–property differences between metallic MoS_2 and semiconducting MoS_2 , the fabrication progress of metallic MoS_2 , and the corresponding applications of metallic phase on lithium-ion batteries, sodium-ion batteries, supercapacitors, and hydrogen evolution reaction. The emphasis of this review is to present the significance of the exceptional intrinsic conductivity and high amount of active sites of metallic MoS_2 , and to cover the superiority of using metallic MoS_2 on high performance energy storage and conversion. The detailed discussion on the high intrinsic conductivity of metallic MoS_2 , especially under high current densities in lithium-ion and sodium-ion batteries, will provide inspiration for designing high rate energy storage device.

Metallic MoS_2 has attracted broad attention for their applications on energy storage and conversion due to its promising properties and the emerging scaleable fabrication methods. Benefitting from its different Mo and S atom coordination of octahedral structure with dense active sites, metallic phase MoS_2 owns the electrical conductivity of five orders magnitude higher than that of semiconducting MoS_2 . This highly conductive metallic MoS_2 will combine the advantages of the individual building blocks while eliminating the associated shortcomings, leading to the expansion of current energy storage

technologies. This review has not only exhibited the enhanced performance of metallic conducting MoS_2 with large current density, but also constructed the fundamental science needed for advanced applications on energy storage and conversion.

In the future, efforts are needed to investigate the fundamentals and develop more controllable fabrication methods, and following aspects are suggested to be paid more attention: 1) the parameters which affect the metallic structure stability should be further investigated. In this review paper, we introduced a way to increase the stability by assembling the metallic MoS_2 nanosheets to hollow tube and to reduce the restacking of the layered nanosheets for its applications on lithium ion battery. Also, we introduced the strategies of coupling a monolayer of water at the nanosheets surface to reduce the restacking and further stabilize the metallic phase and use them for hydrogen evolution reaction and ultrafast supercapacitor. However, metallic phase is also sensitive to pH, light, electron beam, heat, etc., therefore, a further study in this direction will be expected; 2) Controllable synthesis process and applications of metallic MoS_2 are required. In addition to the energy storage and energy conversion, the application of MoS_2 in sensors, electronics, and biomedicine is needed; 3) Further modified methods for stabilized metallic MoS_2 should also be developed. So far, with the autoclave methods, the stability of metallic MoS_2 could be kept for around three months in air, but it is still not stable under higher temperature ($>200 \text{ }^\circ\text{C}$), or radiation. 4) Functionalization of metallic MoS_2 should be explored. Given that the research for metallic MoS_2 on energy storage and conversion has just begun, there are still a lot of studies to be done, and these studies can also be generalized to other 2D TMD materials, such as metallic MoSe_2 , WS_2 , or CoS_2 , which will offer more interesting applications on energy storage and energy conversion in the future.

Acknowledgements

H.L.Z. acknowledges the financial startup support and Tier 1 support from Northeastern University. Y.C.J. acknowledges the financial support of 2016M602669 from CPSF.

Conflict of Interest

The authors declare no conflict of interest.

Keywords

band structures, characterization, energy storage and conversion, fabrication, metallic MoS_2

Received: February 14, 2018

Revised: May 8, 2018

Published online:

[1] M. Chhowalla, H. S. Shin, G. Eda, L. J. Li, K. P. Loh, H. Zhang, *Nat. Chem.* **2013**, *5*, 263.

[2] D. Jariwala, V. K. Sangwan, L. J. Lauhon, T. J. Marks, M. C. Hersam, *ACS Nano* **2014**, *8*, 1102.

- [3] B. W. H. Baugher, H. O. H. Churchill, Y. F. Yang, P. Jarillo-Herrero, *Nat. Nanotechnol.* **2014**, *9*, 262.
- [4] C. L. Tan, H. Zhang, *Chem. Soc. Rev.* **2015**, *44*, 2713.
- [5] H. Li, J. M. T. Wu, Z. Y. Yin, H. Zhang, *Acc. Chem. Res.* **2014**, *47*, 1067.
- [6] M. M. Ugeda, A. J. Bradley, S. F. Shi, F. H. da Jornada, Y. Zhang, D. Y. Qiu, W. Ruan, S. K. Mo, Z. Hussain, Z. X. Shen, F. Wang, S. G. Louie, M. F. Crommie, *Nat. Mater.* **2014**, *13*, 1091.
- [7] G. R. Bhimanapati, Z. Lin, V. Meunier, Y. Jung, J. Cha, S. Das, D. Xiao, Y. Son, M. S. Strano, V. R. Cooper, L. B. Liang, S. G. Louie, E. Ringe, W. Zhou, S. S. Kim, R. R. Naik, B. G. Sumpter, H. Terrones, F. N. Xia, Y. L. Wang, J. Zhu, D. Akinwande, N. Alem, J. A. Schuller, R. E. Schaak, M. Terrones, J. A. Robinson, *ACS Nano* **2015**, *9*, 11509.
- [8] A. Allain, J. H. Kang, K. Banerjee, A. Kis, *Nat. Mater.* **2015**, *14*, 1195.
- [9] D. Lembke, S. Bertolazzi, A. Kis, *Acc. Chem. Res.* **2015**, *48*, 100.
- [10] T. Stephenson, Z. Li, B. Olsen, D. Mitlin, *Energy Environ. Sci.* **2014**, *7*, 209.
- [11] X. Cao, Y. Shi, W. Shi, X. Rui, Q. Yan, J. Kong, H. Zhang, *Small* **2013**, *9*, 3433.
- [12] M. Chhowalla, G. A. J. Amaratunga, *Nature* **2000**, *407*, 164.
- [13] J. N. Coleman, M. Lotya, A. O'Neill, S. D. Bergin, P. J. King, U. Khan, K. Young, A. Gaucher, S. De, R. J. Smith, I. V. Shvets, S. K. Arora, G. Stanton, H.-Y. Kim, K. Lee, G. T. Kim, G. S. Duesberg, T. Hallam, J. J. Boland, J. J. Wang, J. F. Donegan, J. C. Grunlan, G. Moriarty, A. Shmeliov, R. J. Nicholls, J. M. Perkins, E. M. Grieveson, K. Theuvsissen, D. W. McComb, P. D. Nellist, V. Nicolosi, *Science* **2011**, *331*, 568.
- [14] D. S. Kong, H. T. Wang, J. J. Cha, M. Pasta, K. J. Koski, J. Yao, Y. Cui, *Nano Lett.* **2013**, *13*, 1341.
- [15] H. Li, C. Tsai, A. L. Koh, L. Cai, A. W. Contryman, A. H. Fragapane, J. Zhao, H. S. Han, H. C. Manoharan, F. Abild-Pedersen, J. K. Nørskov, X. Zheng, *Nat. Mater.* **2016**, *15*, 48.
- [16] J. Wang, C. Luo, T. Gao, A. Langrock, A. C. Mignerey, C. Wang, *Small* **2015**, *11*, 473.
- [17] D. Voiry, M. Salehi, R. Silva, T. Fujita, M. W. Chen, T. Asefa, V. B. Shenoy, G. Eda, M. Chhowalla, *Nano Lett.* **2013**, *13*, 6222.
- [18] S. Jayabal, G. Saranya, J. Wu, Y. Q. Liu, D. S. Geng, X. B. Meng, *J. Mater. Chem., A* **2017**, *5*, 24540.
- [19] X. Y. Yu, L. Yu, X. W. Lou, *Small Methods* **2017**, *1*, 1600020.
- [20] G. Zhang, H. J. Liu, J. H. Qu, J. H. Li, *Energy Environ. Sci.* **2016**, *9*, 1190.
- [21] Z. L. He, W. X. Que, *Appl. Mater. Today* **2016**, *3*, 23.
- [22] X. M. Geng, Y. L. Zhang, Y. Han, J. X. Li, L. Yang, M. Benamara, L. Chen, H. L. Zhu, *Nano Lett.* **2017**, *17*, 1825.
- [23] K. F. Mak, C. Lee, J. Hone, J. Shan, T. F. Heinz, *Phys. Rev. Lett.* **2010**, *105*, 136805.
- [24] K. Lee, H. Y. Kim, M. Lotya, J. N. Coleman, G. T. Kim, G. S. Duesberg, *Adv. Mater.* **2011**, *23*, 4178.
- [25] X. Y. Yu, H. Hu, Y. W. Wang, H. Y. Chen, X. W. Lou, *Angew. Chem., Int. Ed.* **2015**, *54*, 7395.
- [26] X. Y. Yu, Y. Feng, Y. Jeon, B. Guan, X. W. Lou, U. Paik, *Adv. Mater.* **2016**, *28*, 9006.
- [27] Y. W. Wang, L. Yu, X. W. Lou, *Angew. Chem., Int. Ed.* **2016**, *55*, 7423.
- [28] X. Geng, W. Sun, W. Wu, B. Chen, A. Al-Hilo, M. Benamara, H. Zhu, F. Watanabe, J. Cui, T.-p. Chen, *Nat. Commun.* **2016**, *7*, 10672.
- [29] X. M. Geng, Y. C. Jiao, Y. Han, A. Mukhopadhyay, L. Yang, H. L. Zhu, *Adv. Funct. Mater.* **2017**, *27*, 1702998.
- [30] Y. Jiao, A. Mukhopadhyay, Y. Ma, L. Yang, A. M. Hafez, H. Zhu, *Adv. Energy Mater.* **2018**, *8*, 1702779.
- [31] S. Yang, K. Zhang, C. D. Wang, Y. K. Zhang, S. M. Chen, C. Q. Wu, A. Vasileff, S. Z. Qiao, L. Song, *J. Mater. Chem. A* **2017**, *5*, 23704.
- [32] Y. C. Jeong, J. H. Kim, S. H. Kwon, J. Y. Oh, J. Park, Y. Jung, S. G. Lee, S. J. Yang, C. R. Park, *J. Mater. Chem. A* **2017**, *5*, 23909.
- [33] K. Chang, X. Hai, H. Pang, H. Zhang, L. Shi, G. Liu, H. Liu, G. Zhao, M. Li, J. Ye, *Adv. Mater.* **2016**, *28*, 10033.
- [34] Y. Yin, J. Han, Y. Zhang, X. Zhang, P. Xu, Q. Yuan, L. Samad, X. Wang, Y. Wang, Z. Zhang, *J. Am. Chem. Soc.* **2016**, *138*, 7965.
- [35] L. Yang, A. Mukhopadhyay, Y. Jiao, J. Hamel, M. Benamara, Y. Xing, H. Zhu, *J. Mater. Chem.* **2017**, *5*, 25359.
- [36] G. Eda, T. Fujita, H. Yamaguchi, D. Voiry, M. W. Chen, M. Chhowalla, *ACS Nano* **2012**, *6*, 7311.
- [37] M. Acerce, D. Voiry, M. Chhowalla, *Nat. Nanotechnol.* **2015**, *10*, 313.
- [38] H. H. Huang, Y. Cui, Q. Li, C. C. Dun, W. Zhou, W. X. Huang, L. Chen, C. A. Hewitt, D. L. Carroll, *Nano Energy* **2016**, *26*, 172.
- [39] A. P. Nayak, S. Bhattacharyya, J. Zhu, J. Liu, X. Wu, T. Pandey, C. Q. Jin, A. K. Singh, D. Akinwande, J. F. Lin, *Nat. Commun.* **2014**, *5*, 3731.
- [40] R. Ganatra, Q. Zhang, *ACS Nano* **2014**, *8*, 4074.
- [41] A. Arab, Q. L. Li, *Sci. Rep.* **2015**, *5*, 13706.
- [42] B. Radisavljevic, A. Radenovic, J. Brivio, V. Giacometti, A. Kis, *Nat. Nanotechnol.* **2011**, *6*, 147.
- [43] J. Jia, F. J. Xu, S. L. Wang, X. Jiang, Z. Long, X. D. Hou, *Analyst* **2014**, *139*, 3533.
- [44] S. Balendhran, J. Z. Ou, M. Bhaskaran, S. Sriram, S. Ippolito, Z. Vasic, E. Kats, S. Bhargava, S. Zhuiykov, K. Kalantar-zadeh, *Nanoscale* **2012**, *4*, 461.
- [45] A. Kuc, *Chem. Modell.* **2015**, *11*, 1.
- [46] G. P. Gao, Y. Jiao, F. X. Ma, Y. L. Jiao, E. Waclawik, A. J. Du, *J. Phys. Chem. C* **2015**, *119*, 13124.
- [47] D. Voiry, A. Mohite, M. Chhowalla, *Chem. Soc. Rev.* **2015**, *44*, 2702.
- [48] W. Choi, N. Choudhary, G. H. Han, J. Park, D. Akinwande, Y. H. Lee, *Mater. Today* **2017**, *20*, 116.
- [49] F. X. Ma, G. P. Gao, Y. L. Jiao, Y. T. Gu, A. Bilic, H. J. Zhang, Z. F. Chen, A. J. Du, *Nanoscale* **2016**, *8*, 4969.
- [50] G. Eda, H. Yamaguchi, D. Voiry, T. Fujita, M. W. Chen, M. Chhowalla, *Nano Lett.* **2011**, *11*, 5111.
- [51] D. Y. Qiu, F. H. da Jornada, S. G. Louie, *Phys. Rev. Lett.* **2013**, *111*, 216805.
- [52] Z. Y. Zhu, Y. C. Cheng, U. Schwingenschlogl, *Phys. Rev. B* **2011**, *84*, 153402.
- [53] I. Song, C. Park, H. C. Choi, *RSC Adv.* **2015**, *5*, 7495.
- [54] X. F. Qian, J. W. Liu, L. Fu, J. Li, *Science* **2014**, *346*, 1344.
- [55] K. M. Fair, M. J. Ford, *Nanotechnology* **2015**, *26*, 435705.
- [56] X. Li, H. W. Zhu, *J. Materiomics* **2015**, *1*, 33.
- [57] A. P. Nayak, T. Pandey, D. Voiry, J. Liu, S. T. Moran, A. Sharma, C. Tan, C. H. Chen, L. J. Li, M. Chhowalla, J. F. Lin, A. K. Singh, D. Akinwande, *Nano Lett.* **2015**, *15*, 346.
- [58] M. X. Ye, D. Winslow, D. Y. Zhang, R. Pandey, Y. K. Yap, *Photonics* **2015**, *2*, 288.
- [59] A. Splendiani, L. Sun, Y. B. Zhang, T. S. Li, J. Kim, C. Y. Chim, G. Galli, F. Wang, *Nano Lett.* **2010**, *10*, 1271.
- [60] D. Voiry, A. Goswami, R. Kappera, C. D. C. E. Silva, D. Kaplan, T. Fujita, M. W. Chen, T. Asefa, M. Chhowalla, *Nat. Chem.* **2015**, *7*, 45.
- [61] W. J. Zhao, R. M. Ribeiro, G. Eda, *Acc. Chem. Res.* **2015**, *48*, 91.
- [62] A. Ejigu, I. A. Kinloch, E. Prestat, R. A. W. Dryfe, *J. Mater. Chem. A* **2017**, *5*, 11316.
- [63] C. L. Tan, W. Zhao, A. Chaturvedi, Z. Fei, Z. Y. Zeng, J. Z. Chen, Y. Huang, P. Ercius, Z. M. Luo, X. Y. Qi, B. Chen, Z. C. Lai, B. Li, X. Zhang, J. Yang, Y. Zong, C. H. Jin, H. M. Zheng, C. Kloc, H. Zhang, *Small* **2016**, *12*, 1866.
- [64] M. A. Py, R. R. Haering, *Can. J. Phys.* **1983**, *61*, 76.
- [65] M. A. Lukowski, A. S. Daniel, F. Meng, A. Forticaux, L. S. Li, S. Jin, *J. Am. Chem. Soc.* **2013**, *135*, 10274.
- [66] Q. Ding, F. Meng, C. R. English, M. Caban-Acevedo, M. J. Shearer, D. Liang, A. S. Daniel, R. J. Hamers, S. Jin, *J. Am. Chem. Soc.* **2014**, *136*, 8504.

- [67] Q. Fu, B. Xiang, *Prog. Nat. Sci.: Mater. Int.* **2016**, *26*, 221.
- [68] J. N. Coleman, M. Lotya, A. O'Neill, S. D. Bergin, P. J. King, U. Khan, K. Young, A. Gaucher, S. De, R. J. Smith, I. V. Shvets, S. K. Arora, G. Stanton, H. Y. Kim, K. Lee, G. T. Kim, G. S. Duesberg, T. Hallam, J. J. Boland, J. J. Wang, J. F. Donegan, J. C. Grunlan, G. Moriarty, A. Shmeliov, R. J. Nicholls, J. M. Perkins, E. M. Grievson, K. Theuwissen, D. W. McComb, P. D. Nellist, V. Nicolosi, *Science* **2011**, *331*, 568.
- [69] H. T. Wang, Z. Y. Lu, S. C. Xu, D. S. Kong, J. J. Cha, G. Y. Zheng, P. C. Hsu, K. Yan, D. Bradshaw, F. B. Prinz, Y. Cui, *Proc. Natl. Acad. Sci. USA* **2013**, *110*, 19701.
- [70] L. Cai, J. F. He, Q. H. Liu, T. Yao, L. Chen, W. S. Yan, F. C. Hu, Y. Jiang, Y. D. Zhao, T. D. Hu, Z. H. Sun, S. Q. Wei, *J. Am. Chem. Soc.* **2015**, *137*, 2622.
- [71] T. Xiang, Q. Fang, H. Xie, C. Q. Wu, C. D. Wang, Y. Zhou, D. B. Liu, S. M. Chen, A. Khalil, S. Tao, Q. Liu, L. Song, *Nanoscale* **2017**, *9*, 6975.
- [72] Q. Liu, Q. Fang, W. S. Chu, Y. Y. Wan, X. L. Li, W. Y. Xu, M. Habib, S. Tao, Y. Zhou, D. B. Liu, T. Xiang, A. Khalil, X. J. Wu, M. Chhowalla, P. M. Ajayan, L. Song, *Chem. Mater.* **2017**, *29*, 4738.
- [73] M. Wu, J. Zhan, K. Wu, Z. Li, L. Wang, B. Geng, L. Wang, D. Pan, *J. Mater. Chem. A* **2017**, *5*, 14061.
- [74] S. Bai, L. M. Wang, X. Y. Chen, J. T. Du, Y. J. Xiong, *Nano Res.* **2015**, *8*, 175.
- [75] Q. Liu, X. L. Li, Q. He, A. Khalil, D. B. Liu, T. Xiang, X. J. Wu, L. Song, *Small* **2015**, *11*, 5556.
- [76] Y. C. Lin, D. O. Dumcenco, H. P. Komsa, Y. Niimi, A. V. Krasheninnikov, Y. S. Huang, K. Suenaga, *Adv. Mater.* **2014**, *26*, 2857.
- [77] L. F. Wang, Z. Xu, W. L. Wang, X. D. Bai, *J. Am. Chem. Soc.* **2014**, *136*, 6693.
- [78] S. J. Sandoval, D. Yang, R. F. Frindt, J. C. Irwin, *Phys. Rev. B* **1991**, *44*, 3955.
- [79] X. B. Fan, P. T. Xu, D. K. Zhou, Y. F. Sun, Y. G. C. Li, M. A. T. Nguyen, M. Terrones, T. E. Mallouk, *Nano Lett.* **2015**, *15*, 5956.
- [80] M. K. Jana, C. N. R. Rao, *Philos. Trans. R. Soc., A* **2016**, *374*, 20150318.
- [81] J. J. Wu, M. J. Liu, K. Chatterjee, K. P. Hackenberg, J. F. Shen, X. L. Zou, Y. Yan, J. Gu, Y. C. Yang, J. Lou, P. M. Ajayan, *Adv. Mater. Interfaces* **2016**, *3*, 1500669.
- [82] P. Joensen, E. D. Crozier, N. Alberding, R. F. Frindt, *J. Phys. C: Solid State Phys.* **1987**, *20*, 4043.
- [83] R. Kappera, D. Voiry, S. E. Yalcin, B. Branch, G. Gupta, A. D. Mohite, M. Chhowalla, *Nat. Mater.* **2014**, *13*, 1128.
- [84] K. Chang, W. X. Chen, *ACS Nano* **2011**, *5*, 4720.
- [85] H. Hwang, H. Kim, J. Cho, *Nano Lett.* **2011**, *11*, 4826.
- [86] Y. M. Chen, X. Y. Yu, Z. Li, U. Paik, X. W. Lou, *Sci. Adv.* **2016**, *2*, e1600021.
- [87] Y. P. Liu, X. Y. He, D. Hanlon, A. Harvey, U. Khan, Y. G. Li, J. N. Coleman, *ACS Nano* **2016**, *10*, 5980.
- [88] X. H. Cao, C. L. Tan, X. Zhang, W. Zhao, H. Zhang, *Adv. Mater.* **2016**, *28*, 6167.
- [89] M. Winter, R. J. Brodd, *Chem. Rev.* **2004**, *104*, 4245.
- [90] H. Tang, J. Wang, H. Yin, H. Zhao, D. Wang, Z. Tang, *Adv. Mater.* **2015**, *27*, 1117.
- [91] J. Feng, X. Sun, C. Wu, L. Peng, C. Lin, S. Hu, J. Yang, Y. Xie, *J. Am. Chem. Soc.* **2011**, *133*, 17832.
- [92] J. Zhu, W. Sun, D. Yang, Y. Zhang, H. H. Hoon, H. Zhang, Q. Yan, *Small* **2015**, *11*, 4123.
- [93] S. Zhu, X. Geng, Y. Han, M. Benamara, L. Chen, J. Li, I. Bilgin, H. Zhu, *npj Comput. Mater.* **2017**, *3*, 41.
- [94] J. Xiao, D. Choi, L. Cosimbescu, P. Koech, J. Liu, J. P. Lemmon, *Chem. Mater.* **2010**, *22*, 4522.
- [95] J. Zheng, H. Zhang, S. Dong, Y. Liu, C. Tai Nai, H. Suk Shin, H. Young Jeong, B. Liu, K. Ping Loh, *Nat. Commun.* **2014**, *5*, 2995.
- [96] G. W. Crabtree, M. S. Dresselhaus, M. V. Buchanan, *Physics Today* **2004**, *57*, 39.
- [97] J. Greeley, T. F. Jaramillo, J. Bonde, I. B. Chorkendorff, J. K. Norskov, *Nat. Mater.* **2006**, *5*, 909.
- [98] Q. P. Lu, Y. F. Yu, Q. L. Ma, B. Chen, H. Zhang, *Adv. Mater.* **2016**, *28*, 1917.
- [99] M. S. Faber, S. Jin, *Energy Environ. Sci.* **2014**, *7*, 3519.
- [100] A. Hagfeldt, G. Boschloo, L. C. Sun, L. Kloo, H. Pettersson, *Chem. Rev.* **2010**, *110*, 6595.
- [101] Y. Okamoto, S. Ida, J. Hyodo, H. Hagiwara, T. Ishihara, *J. Am. Chem. Soc.* **2011**, *133*, 18034.
- [102] S. Cobo, J. Heidkamp, P. A. Jacques, J. Fize, V. Fourmond, L. Guetaz, B. Jousset, V. Ivanova, H. Dau, S. Palacin, M. Fontecave, V. Artero, *Nat. Mater.* **2012**, *11*, 802.
- [103] D. J. Evans, C. J. Pickett, *Chem. Soc. Rev.* **2003**, *32*, 268.
- [104] H. I. Karunadasa, C. J. Chang, J. R. Long, *Nature* **2010**, *464*, 1329.
- [105] M. L. Helm, M. P. Stewart, R. M. Bullock, M. R. DuBois, D. L. DuBois, *Science* **2011**, *333*, 863.
- [106] D. S. Kong, J. J. Cha, H. T. Wang, H. R. Lee, Y. Cui, *Energy Environ. Sci.* **2013**, *6*, 3553.
- [107] B. Hinnemann, P. G. Moses, J. Bonde, K. P. Jorgensen, J. H. Nielsen, S. Horch, I. Chorkendorff, J. K. Norskov, *J. Am. Chem. Soc.* **2005**, *127*, 5308.
- [108] T. F. Jaramillo, K. P. Jorgensen, J. Bonde, J. H. Nielsen, S. Horch, I. Chorkendorff, *Science* **2007**, *317*, 100.
- [109] Y. Jiao, Y. Zheng, M. T. Jaroniec, S. Z. Qiao, *Chem. Soc. Rev.* **2015**, *44*, 2060.
- [110] C. K. Chua, A. H. Loo, M. Pumera, *Chem. - Eur. J.* **2016**, *22*, 14336.
- [111] L. L. Wang, X. Liu, J. M. Luo, X. D. Duan, J. Crittenden, C. B. Liu, S. Q. Zhang, Y. Pei, Y. X. Zeng, X. F. Duan, *Angew. Chem., Int. Ed.* **2017**, *56*, 7610.
- [112] X. Zhao, X. Ma, Q. Q. Lu, Q. Li, C. Han, Z. C. Xing, X. R. Yang, *Electrochim. Acta* **2017**, *249*, 72.
- [113] U. Maitra, U. Gupta, M. De, R. Datta, A. Govindaraj, C. N. R. Rao, *Angew. Chem., Int. Ed.* **2013**, *52*, 13057.
- [114] Q. Liu, Q. C. Shang, A. Khalil, Q. Fang, S. M. Chen, Q. He, T. Xiang, D. B. Liu, Q. Zhang, Y. Luo, L. Song, *ChemCatChem* **2016**, *8*, 2614.
- [115] K. Chang, X. Hai, H. Pang, H. B. Zhang, L. Shi, G. G. Liu, H. M. Liu, G. X. Zhao, M. Li, J. H. Ye, *Adv. Mater.* **2016**, *28*, 10033.
- [116] Y. Li, L. L. Wang, S. Q. Zhang, X. R. Dong, Y. Z. Song, T. Cai, Y. T. Liu, *Catal. Sci. Technol.* **2017**, *7*, 718.
- [117] X. B. Li, Y. J. Gao, H. L. Wu, Y. Wang, Q. Guo, M. Y. Huang, B. Chen, C. H. Tung, L. Z. Wu, *Chem. Commun.* **2017**, *53*, 5606.